Universidade de Aveiro
2023

Guilherme Simões de Sá Reis

Optimization of heat transfer in Phase Change Materials using metallic porous structures

Otimização da transferência de calor em Materiais de Mudança de Fase com recurso a estruturas porosas metálicas

Universidade de Aveiro
2023

Guilherme Simões de Sá Reis

Optimization of heat transfer in Phase Change Materials using metallic porous structures

Otimização da transferência de calor em Materiais de Mudança de Fase com recurso a estruturas porosas metálicas

Dissertação apresentada à Universidade de Aveiro para cumprimento dos requisitos necessários à obtenção do grau de Mestre em Engenharia Mecânica, realizada sob orientação científica de Fernando José Neto da Silva, Professor Auxiliar, do Departamento de Engenharia Mecânica da Universidade de Aveiro.

Esta dissertação teve o apoio dos projectos UIDB/00481/2020 e UIDP/00481/2020 - Fundação para a Ciência e Tecnologia; e CENTRO-01-0145 FEDERCap3-022083 - Programa Operacional Regional do Centro (Centro2020), através do Portugal e do Fundo Europeu de Desenvolvimento Regional

O júri / **The jury**

Presidente / President

Prof. Doutor Vítor António Ferreira da Costa
Professor Catedrático da Universidade de Aveiro

Vogais / Committee

Prof. Doutor José Joaquim da Costa
Professor Associado da *Universidade de Coimbra*

Prof. Doutor Fernando José Neto da Silva
Professor Auxiliar da Universidade de Aveiro

Agradecimentos /
Acknowledgements

First and foremost, I would like to express my deepest gratitude to my parents and brother for their unwavering support throughout my academic journey, without which none of this would have been possible.
I am also immensely grateful to Daniel Marques and Mariana Conde, both PhD students from the Department of Mechanical Engineering at the University of Aveiro, whose invaluable assistance and guidance were instrumental in the development of this dissertation and its contents. Their expertise and dedication have greatly contributed to the overall quality of this work.
Also, I would like to acknowledge nTopology for providing their software nTop. Without it, these dissertations models could not have been so promptly created and tested.
Finally, I express my gratitude to Professor Fernando for his support throughout the development process of this project.

Keywords

Phase Change Materials, Thermal Energy Storage, cell size optimization, thickness optimization, lattice structures, performance enhancement, heat storage capacity, metal matrix, PCM, TES

Abstract

Phase change materials (PCM) for use in Thermal Energy Storage (TES) systems have garnered significant attention in recent years. However, the limited thermal conductivity of PCM remains a major challenge. To address this issue, various techniques have been explored, ranging from the use of multiple PCM to lattice systems. The latter, particularly, has gained popularity as a promising method to enhance PCM for TES, offering superior thermal enhancement capabilities.

This thesis explores the optimization of cell size and thickness parameters in lattice systems using PCM for TES. The objective is to enhance system performance and heat storage capacity through simulation methodology development and parameter optimization.

A robust simulation methodology is developed using nTop and Ansys® software to analyze various lattice structures (Kelvin, IsoTruss, and Gyroid) combined with PCM. The focus then shifts to optimizing cell size and thickness parameters within the lattice structure, which impact PCM volume, surface area, performance, and convergence rate.

Increasing the thickness of the structure improves system performance by 68% but decreases heat storage capacity by 10%. Decreasing thickness has a detrimental effect, reducing performance by 347% but increasing heat storage capacity by 9%. Increasing cell size modestly improves performance by 3% and slightly increases heat storage capacity by 1%. Decreasing cell size yields mixed results, with enhanced performance in some structures and a consistent average decrease of 3% in heat storage capacity.

These findings highlight the importance of careful parameter selection and the sensitivity of different lattice structures to changes in cell size and thickness. A systematic approach to parameter optimization is necessary to achieve optimal performance. By identifying the optimal combination of parameters, significant enhancements in performance, convergence rate, and heat storage capacity can be achieved.

Palavras-chave

Materiais de Mudança de Fase, Armazenamento de Energia Térmica, otimização do tamanho da célula, estruturas de rede, melhoria de desempenho, capacidade de armazenamento de calor, matriz de metal, PCM, TES

Resumo

Materiais de mudança de fase (PCM) para uso em sistemas de Armazenamento de Energia Térmica (TES) têm recebido atenção significativa nos últimos anos. No entanto, a limitada condutividade térmica dos PCM continua a ser um desafio importante. Para enfrentar esta questão, várias técnicas têm sido exploradas, desde o uso de múltiplos PCM até sistemas de treliça. Este último, em particular, tem ganhado popularidade como um método promissor para melhorar os PCM para TES, oferecendo capacidades superiores de aprimoramento térmico.

Esta dissertação explora a otimização do tamanho de célula e espessura em sistemas de treliça usando PCM para TES. O objetivo é aprimorar o desempenho do sistema e a capacidade de armazenamento de calor por meio do desenvolvimento de metodologia de simulação e otimização de parâmetros.

Uma metodologia de simulação robusta é desenvolvida usando os softwares nTop e Ansys® para analisar diversas estruturas de lattice (Kelvin, IsoTruss e Gyroid) combinadas com PCM. O foco então vira-se para a otimização dos parâmetros de tamanho de célula e espessura dentro da estrutura de treliça, que afetam o volume do PCM, área superficial, desempenho e taxa de convergência.

Em média, aumentar a espessura da estrutura melhora o desempenho do sistema em 68%, mas diminui a capacidade de armazenamento de calor em 10%. Diminuir a espessura tem um efeito prejudicial, reduzindo o desempenho em 347%, mas aumentando a capacidade de armazenamento de calor em 9%. Aumentar o tamanho da célula melhora modestamente o desempenho em 3% e aumenta ligeiramente a capacidade de armazenamento de calor em 1%. Diminuir o tamanho da célula produz resultados mistos, com melhoria de desempenho em algumas estruturas e uma diminuição média consistente de 3% na capacidade de armazenamento de calor.

Esses resultados destacam a importância da seleção cuidadosa de parâmetros e a sensibilidade de diferentes estruturas de treliça a alterações no tamanho da célula e na espessura. Uma abordagem sistemática para a otimização de parâmetros é necessária para alcançar um desempenho ótimo. Ao identificar a combinação ideal de parâmetros, podem ser obtidos aprimoramentos significativos no desempenho, taxa de convergência e capacidade de armazenamento de calor.

Contents

List of Tables

Intentionally blank page.

List of Figures

Intentionally blank page.

Nomenclature

β	Thermal expansion coeficient [K^{-1}]
η	Dynamic Viscosity [kg m$^{-1}s^{-1}$]
ρ	Density [kg m^{-3}]
c_p	Specific heat capacity [J kg$^{-1}K^{-1}$]
k	Thermal conductivity [W m$^{-1}K^{-1}$]
L	Heat storage capacity [J kg^{-1}]
T_l	Solidification Temperature [K]
T_s	Melting temperature [K]

Intentionally blank page.

Chapter 1

Introduction

1.1 Introduction

Humanity's continuous progress is made possible through the use of different types of energy. Up until the twentieth-century energy sources were primarily sourced from non-renewable kinds. Despite this, throughout the years, the emerging threat of energy and climate crisis has shifted the paradigm and renewable sources are being pushed as the correct and sustainable way to pave the future. According to the International Energy Agency [10], it is estimated that between 2021 and 2030 investment in clean forms of energy will increase from around 1.12 trillion euros to 1.96 trillion euros whilst the use of fossil fuels, which has been around 80% worldwide for decades, is expected to drop to 75% by 2030 and as low as 60% by 2050.

In a context where non-renewable energy sources are becoming less and less desirable, renewable ones become the future solution for the energy problem worldwide. One of the drawbacks regarding renewable energy however is its availability. Oftentimes these sources are not available at the time of need so energy storage is a vital technology for the viability of some energy sources. Energy storage is essentially the capture of energy at a single point in time for use in the future. It can be achieved by implementing a variety of technologies and means such as mechanical, magnetic, chemical and thermal.

Expanding on the latter, Thermal Energy Storage (TES) Systems possess low construction cost, high energy density, and the ability to store energy directly. These systems are achievable in three forms: i) Sensible heat storage (SHS) in which the temperature of a storage medium is made to increase or decrease by its surrounding environment; the stored energy has a linear relationship with temperature and will highly depend on the specific heat capacity of the material used, typically water, oil or ceramic materials [11]. This type of TES is commonly used in industrial applications, residential water heaters, or hot water storage on district-heating networks. The main drawback of this system is its low energy density and likely loss of thermal energy at any temperature, although building materials with high thermal capacity will allow for thermal storage for up to some months; ii) Latent heat storage (LHS) which utilizes the heat transfer occurring during the phase change of a material within a narrow temperature range. To achieve this, specific materials are used, such as molten salt, paraffin wax, oils, or water/ice. This phase transition can happen as solid-liquid meaning melting and freezing, liquid-gas meaning evaporation and condensation or even solid-solid in which changes to the crystalline structure of the material happen while the temperature is tailored to the specific material. This TES system makes use of the rearranging of the chemical bonds of the material used to generate heat and thus provides a very high thermal energy storage density proving to be more efficient when compared

to SHS; iii) Thermochemical storage (TCS) utilizes a reversible endothermic chemical reaction that, through strong chemical bonds, stores energy as chemical potential. An energy-consuming reaction stores energy, and when required, the reverse reaction recombines the chemical reactants and releases energy. Out of the three TES technologies, TCS theoretically provides higher energy density with minimum energy loss over long periods. This is not without its issues, TCS systems seem to have stability problems and appear to not have constant efficiency over time. [11]

Recently, there has been a growing interest in using Phase Changing Materials (PCM) in Latent Heat Thermal Storage (LHS) systems. These materials have the ability to absorb and release large amounts of thermal energy during their phase transition, within a specific temperature range. However, outside of this range, they may only exchange typical sensible heat. This has led to the use of PCM in a variety of fields such as thermal energy storage [12, 13], batteries [14, 15], aerospace [16, 17], textiles [18, 19], and photovoltaics [14, 20]. In particular, PCM are commonly used as thermal storage tanks for industrial processes [21], buildings [22, 23], agriculture [24], and fuel cells [25,26]. PCM can be effectively applied in thermal regulation [27] and storage systems, and are particularly promising for thermal regulation of buildings and space air conditioning [28, 29] as they can mitigate large temperature fluctuations. Furthermore, PCM that undergo phase transitions around the human comfort zone temperatures (10-25ºC) can help save energy when used to regulate the temperature in living spaces. [11]

The various PCM can be subdivided into three categories depending on the material composition: organic, such as paraffins, fatty acids and polyethylene glycol (PEG), inorganic, such as salt hydrates and nitrates, and eutectic, which consists of the combination of 2 or more PCM. Also, PCM can be divided into two more categories according to their melting temperature: below 200ºC are low-temperature and above 200ºC are high-temperature PCM. The first ones are mainly used in waste heat recovery systems and buildings and the others are typically used in solar power plants and other high-temperature applications. There are some desirable thermophysical, kinetic and chemical properties. These may include: the melting temperature should be in the range of operating temperature, high latent heat of fusion, high thermal conductivity, high density, low volume change during phase change, low degree of supercooling, low corrosion to the construction materials, low degradation, chemical stability, non-toxic and non-flammable, easily available and cost-effective. In Tables 1.1 and 1.2 comparison between different heat storage mediums can be observed[1]. [30]

1.2 Proposed objective

Although PCM possesses a large capacity for storing and releasing thermal energy within a small temperature variation and using a small volume, with the exception of metallic PCM all of them suffer from having low thermal conductivity (around 0.2 W/mK in paraffin wax and $0.5W/mK$ in inorganic salts). This makes the charging and discharging of thermal energy a time-consuming process. To analyze and try to improve the conductivity of PCM, several studies have been carried out regarding different techniques to augment the thermal response of

[1]Paraffin wax (as solid–liquid PCM) of mass 20.513 kg can store/release 5000 kJ of energy at its melting temperature (59.9°C) by assuming its initial temperature of 35°C. To store the same amount of energy, other sensible heat storage mediums would have to be heated at much higher temperatures as shown in Table 1.2. In Table 1.1, the relative mass and relative volume of each material are calculated based on their respective densities, storage mass and volume and by comparing the result to Paraffin Wax. [1]

Table 1.1: Comparison of various heat storage mediums(stored energy = 5000 kJ, with ΔT = 25) [1].

Property	Heat storage material						
	Paraffin Wax	Water	Downtherm.A	Therminal 66	Cast iron	Rock	Concrete
Latent heat of fusion (kJ/kg)	190	*	*	*	*	*	*
Specific heat (kJ/kgK)	2.15	4.19	2.2	2.1	0.54	0.88	0.882
Density(kg/m^3)	790	1000	867	750	7200	1600	2200
Storage mass(kg)	20.513	47.73	90.91	95.24	370.37	227.27	226.76
Relative mass**	1	2.33	4.43	4.64	18.01	11.08	11.05
Storage volume (m^3)	0.02597	0.04773	0.10485	0.127	0.0514	0.142	0.1031
Relative volume**	1	1.84	4.04	4.89	1.98	5.97	3.969

*Latent heat of fusion is not of interest for sensible heat storage

**Relative mass and volume are based on heat storage in paraffin wax

Table 1.2: Temperatue rise needed to store 5000kJ of energy [1].

Heat Storage Material	Temperature Rise
Paraffin Wax	59.90*
Water	93.17
Downtherm A	145.80
Therminal 66	151.10
Concrete	311.40
Rock	312.00
Cast Iron	486.40

*Melting Temperature

PCM. Among said studies, the use of porous metal foams and lattices appears to stand out as a novel and effective method to enhance PCM.

It is apparent then that research needs to be one in order to understand these methods and techniques and how they stack up against the use of lattices and metal foams. The following literature review will focus on achieving such goal.

Chapter 2

Literature review

Before looking at said methods or techniques on how to improve PCM-based systems it is important to address encapsulation. Generally, when using a Heat Transfer Fluid (HTF) it is of vital importance that the PCM remains contained so that they do not mix. It also helps in the longevity of the system by shielding the PCM from the environment. In this regard, PCM encapsulation is a very relevant matter.

Encapsulation consists in surrounding the PCM in a shell material that protects it. It also increases the heat transfer rate by increasing contact surface area or using a material which has a higher thermal conductivity. This material typically meets requirements such as strength, flexibility to support volume change during phase transition, corrosion resistance and thermal stability [1]. The different types of encapsulation can be distinguished by their capsule size, macro-encapsulation (1-10 mm), micro-encapsulation (1-1000 μm), and nano-encapsulation (less than 1μm) [8]. One example of the encapsulation of PCM is the shell and tube system. Mustafa *et al.* [3] studied different Shell and Tube Heat Exchanger (STHE) configurations visible in Figure 2.1. Here the cross-section of the shell enclosing the PCM is crossed by three tubes containing water which act as a Heat Transfer Fluid. Four different configurations are presented. It was reported that the lower the pipes were located the quicker the energy transfer process would finalize. Patricia Graça [31] later, for configuration B, studied the melting rate and heat transfer in this geometry. According to the author configuration B was chosen because "even though case D was the one *who* developed the shortest total melting time, case B revealed the quickest melting rate for the majority of the simulation time, as well as presented the geometry that is the most consistent with both the STHE principle and the study of the influence of convection flows effect, by having the pipes more spaced and distributed on the geometry in an "upside down triangular shape" [31]. The results showed that the configuration with more of a horizontal component performed better in the evaluated parameters such as malting rate, heat transfer, and liquid fraction. The best-performing option reduced the charging time by 23.48% compared to the original case. The study also found that the proposed solution allowed the system to charge 90% of total capacity in 37.2% less time, making it more suitable for use with renewable energy sources such as solar water systems.

2.1 PCM enhancement Techniques

PCM enhancement techniques are of two types, heat transfer enhancement and thermal conductivity enhancement. The first one is more widely used and consists of methods such as:

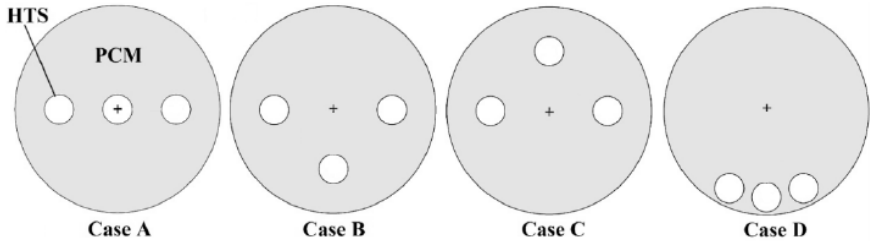

Figure 2.1: Different case studies used in [3].

- Fin configurations,
- Heat Pipes and
- Porous Foams/Matrixes.

The second one,

- Low-density materials with high conductivity,
- Nanoparticles,
- PCM Slurries and
- Use of multiple PCM;

The main difference between these two groups is that the first focuses on increasing the rate at which heat may flow to the PCM whereas the second focuses on increasing the thermal conductivity of the PCM system before engaging with its heat source. Ultimately both strategies work and are very widely studied in the literature, as will be presented. It is also worth noting that the combination of multiple strategies has also been the subject of different studies [32, 33].

2.1.1 Fin configurations

Fin configuration is one of the most widely researched methods to enhance heat transfer to PCM. Consisting in extended surfaces that increase the surface area available for heat transfer, fins have been reported to improve the heat transfer of PCM-based systems. In a study by Akshaykumar *et al.* [4], numerical investigations are conducted to identify the ideal fin arrangement that would lower the thermal control module's critical temperature (T_{cr}). The primary criteria/variables considered were the size, quantity, form, and fin mass percentage. Rectangular, triangular and circular prisms, as well as rectangular, triangular and circular rib pyramids are among the six rib geometries that are studied, as can be seen in Figure 2.2. Results show that T_{cr} declines when using 9 to 100 ribs and that there is no further decline in T_{cr} after that. Comparing prism geometries with the truncated cones, using the corresponding percentage mass of the ribs, it was found that prism geometries had a lower critical temperature.

Two types of fins exist: the first type facilitates the transfer of heat from a fluid to the PCM [32], while the second type enables heat transfer from a wall to the PCM [4]. They can be made from a variety of materials, including metal, plastic, and composite materials, and they can be attached to the surface of the PCM in various configurations. The choice of the fin's material

and configuration can have a significant impact on the performance of the PCM and should be carefully considered. [4]

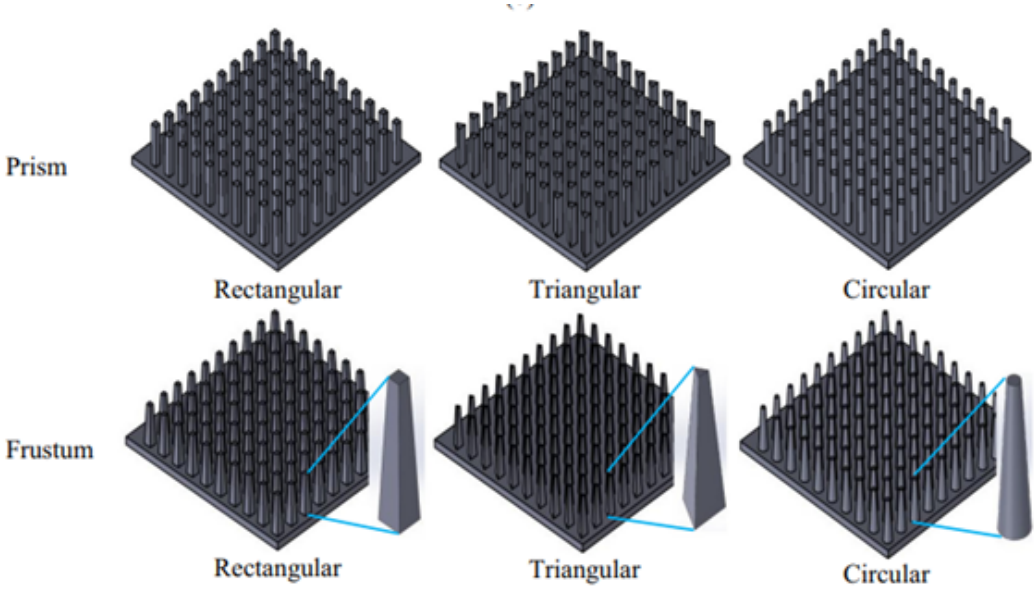

Figure 2.2: Thermal control module having different fin geometries and 100 fins. This includes fin geometries of a rectangular prism, triangular prism, circular prism and rectangular frustum, triangular frustum, circular frustum [4].

2.1.2 Heat Pipes

Heat pipes (HP) serve as a thermal carrier between the HTF and PCM. In particular, in systems involving cyclic charging and discharging, such as cooling and heating, energy recovery, and heat sink devices, the use of HP in LHTES systems is a promising and significant technology for speeding up the charging and discharging operations of PCM. Heat pipes come in a variety of designs and work passively in a certain temperature range [34]. The two main forms of heat pipes are wickless or gravity-assisted and wick-assisted or screen mesh heat pipes, both of which operate with a variety of working fluids [35].

The operating temperature range, size, and geometrical configuration of the storage system all influence the choice of HP type and working fluid for thermal energy storage augmentation. The shell-and-tube structure is a typical storage method that works well with HPs to improve heat transfer. Nithyanandam and Pitchumani [36] carried out an investigation to assess the impact of the number, orientation, and design of HPs on the thermal performance of an LHTES system. The efficiency of the HP-embedded designs was calculated using a 3D computational study, taking both melting (charging) and solidification (discharging) into account. A model using 4 HP, performed better in terms of effectiveness while both charging and discharging, according to the data.

2.1.3 Use of multiple PCM

One peculiar technique suggested in the literature is the use of multiple families of PCM which sometimes is addressed as cascade storage [8]. The purpose of multiple PCM is to keep the

temperature difference between the HTF and the PCM nearly constant during charging and discharging cycles, thereby improving the thermal performance of the LHTES system. During the charging process of a typical shell-and-tube LHTES system, multiple PCM with different melting temperatures are arranged in decreasing order of their melting points along the flow direction of HTF, as shown in Figure 2.3. This trend results in a nearly constant heat flux to the PCM. During the discharging cycle, the HTF flow direction is reversed, so the PCM remain in the increasing order of their melting points and a nearly constant heat flux from PCM to HTF can be obtained [5, 37].

Figure 2.3: Schematic of multiple PCM in shell-and-tube LHTES unit adapted from [5].

2.1.4 Low-density materials with high conductivity

Insertion of high thermal conductivity materials, such as metallic particles, is a common way to enhance PCM-based systems' thermal performance. However, these materials often have high densities which in turn leads to their settlement at the bottom surface of the PCM container [8, 38]. Because of this, materials with low density and high conductivity have been studied as an alternative. Low-density materials have low heat capacities, which can help to reduce the weight of the system while still providing good thermal performance. One example of this is carbon fibres. This material is known for its high thermal conductivity and low thermal expansion, making them a suitable candidate for use with PCM. The integration of carbon fibres can improve thermal performance by facilitating rapid heat transfer and reducing thermal stress. They can also be used as reinforcement in PCM composites, which can increase their mechanical strength and stability during thermal cycling, and enhance the thermal conductivity of the PCM, making them more effective at storing and releasing thermal energy.

2.1.5 Nano particles

Significant progress in the use of high-conductivity nano-materials combined with PCM to enhance their thermal conductivity has been achieved recently. This includes the use of nanopowders (such as Al, CuO, Cu, SiC), nanowires (NW) and carbon nanotubes (CNT) [5]. Nanoparticles embedded into conventional PCM exhibit a better thermal conductivity in comparison to the base material as seen in a study by Khodadadi and Hosseinizadeh [39]. Improvement of the heat transfer efficiency and reduction of the melting and solidification times is another benefit to these systems. Mettawee and Assassa [38] studied the effect of aluminum powder on the thermal conductivity enhancement of paraffin wax in a compact PCM solar collector. The experimental results showed that adding aluminum powder to the wax reduced charging time by about 60%. When the aluminum powder was added to the wax during the discharging process, the useful heat gained was increased when compared to pure paraffin wax. Jegadheeswaran and Pohekar [40] investigated how a shell and tube storage unit dispersed with high-conductivity

copper particles could improve performance. Their results showed that adding particles with a volume fraction of 0.1 reduced discharging time by approximately 28% and particles with a volume fraction of 0.6 reduced discharging time by approximately 85%. The results also revealed an increase in the unit's exergy efficiency of 12% with 0.1 vol fraction and 40% with 0.4 vol fraction. [5]

2.1.6 Phase change slurries

Phase change slurries are binary systems composed of a carrier fluid, typically water, as the continuous phase and a PCM as the dispersed phase. Phase change slurries store or transfer thermal energy by utilizing the PCM latent heat capacity, as well as, the sensible heat capacities of the carrier fluid and the PCM [41]. By using micro/nano-encapsulated PCM slurries, the heat capacity and heat transfer rate of heat transfer fluids or storage media can also be enhanced. Yusuf *et al.* [41] compiled a state of the art on various properties of clathrate hydrate slurries, microencapsulated PCM slurries, shape-stabilized PCM slurries, and phase change material emulsions providing relevant information for laboratory and industrial selection of appropriate PCM slurries. Huang *et al.* [42] investigated phase change slurries of paraffin wax mixtures and water emulsions with melting points in the range of 2–12°C and found that paraffin wax/water emulsions with a paraffin mass fraction of 30–50% were suitable for refrigeration and distribution application. [43]

2.1.7 Porous foams/matrixes

Structures incorporating porous foams or matrices allow for the infiltration of phase change materials (PCM) by virtue of the absence or removal of inner material. The use of porous metal matrices offers several advantages. Firstly, they provide a large surface area for efficient heat transfer between the PCM and the surrounding fluid or material, thereby increasing the rate of heat transfer and enhancing the efficiency of the thermal storage system. Secondly, the high thermal conductivity of the matrix material ensures improved thermal performance. Additionally, the porous structure of the metal matrix provides mechanical support and helps prevent PCM leakage or shifting during thermal cycling, similar to encapsulation.

Impregnation of porous materials is a rapidly growing technique to enhance the thermal conductivity of conventional PCM in latent heat thermal energy storage (LHTES) systems. Porous materials have superior heat transfer properties compared to pure PCM [2, 5]. Chen *et al.* [44] demonstrated the impact of a metal foam on the melting rate of a PCM. Their study revealed that the presence of a porous metal foam significantly enhances melting heat transfer, resulting in a higher melting rate, faster melting front evolution, and a greater liquid fraction of PCM compared to PCM alone.

There are two main types of porous matrices: metallic and carbon-based [2, 5, 8]. Metals with high thermal conductivities, such as silver, copper, gold, and aluminum, are commonly used [45]. Copper and aluminum, which are more cost-effective than silver and gold, are often preferred [6, 46]. The selection of the matrix material depends on various factors, including the desired thermal energy storage capacity, operating temperature range, thermal conductivity, and durability. Aluminum is favored for its high thermal conductivity, low density, and formability, while copper is frequently used in applications requiring high heat transfer rate. Stainless steel, known for its corrosion resistance and mechanical strength, is suitable for harsh environments. Nickel, although possessing relatively low thermal conductivity, has a higher melting point than

copper or aluminum, making it suitable for high melting point solutions [2]. Table 2.1 provides properties of these materials.

Table 2.1: Comparison of properties of different foaming materials [2].

Material	$\rho(kg/m3)$	k (W/ m.K)	T_s(K)	Cost ($/$ton$)
Copper	8933	350-401	1359.15	6685
Aluminium	2700	205-230	933.15	1996
Nickel	8907	89	1728.15	11809
Graphite	2266	170	4398.15	1750

In addition to metal foams and matrices, carbon-based foams are also worth mentioning. These foams can be made from carbon, graphite, or expanded graphite (EG). Research by Zhong *et al.* [47] indicates that graphite with smaller pore size and thicker ligaments exhibits higher thermal diffusivity, while a larger pore size and thinner ligament increase the latent heat storage capacity of graphite. Another study by Zhong *et al.* [48] investigated the density of various natural EG matrices and their impact on the performance of a paraffin-based LHTES system. The findings suggest a linear relationship between thermal conductivity, bulk density of expanded natural graphite, latent heat of the composite, mass ratio of paraffin wax, and the expanded natural graphite matrix.

When looking at these two different types, metal versus carbon-based, the metal variant seems to come out for PCM enhancement. A comparative study by Wu and Zhao [49] carried out an experimental investigation into the use of metal foams and EG with NaNO3 as the PCM, under bottom and top heating conditions. It was reported that in the heating of solid NaNO3 the heat transfer rate by use of metal foam, EG and a combination of both was enhanced by 210%, 190% and 250% respectively. When using the PCM in a fluid state however the opposite was verified. The use of these structures impeded the natural convection of the material and consequently the heat transfer performance when using metal foams or EG is lesser when compared with pure NaNO3.

Even after considering the best materials, porosity and cell/pore size, which refer to, respectively, the percentage of the volume that will be occupied by PCM and the size of the pore expressed in pores per cm, appear to be the two factors that define a porous matrix [8]. Khabib *et al.*l [6] monitored the effect of high conductivity aluminium foam on the phase change of paraffin wax. The main objective was to determine how these two different parameters, foam porosity and pore size, affected the melting of paraffin wax and the heat transfer process as a whole. It was determined that by using higher porosity or bigger pore size foams, steady-state temperature was reached faster due to higher convection (see Figure 2.4). In contrast, for foams with lower porosity, the heater temperature was lower due to greater conduction through the material. This study suggests that there might be an optimal value for pore size and density in order to make better use of both convection and conduction.

If there is an ideal value for pore size and density that maximizes conduction and convection there must be a way to develop a system to this effect. One study by Kumar and Saha [32] tests this hypothesis by developing a novel design for a multitube shell and tube latent heat thermal storage system resorting to a variable porosity metal matrix. In this design, the PCM is contained inside the shell and a heat transfer fluid flows through seven tubes with internal fins located inside the Shell. The shell itself is a metal matrix. In this study, it is assumed that the majority of literature focusing on metal matrices as a method for enhancing heat transfer employs a uniform porosity approach, where the porosity remains consistent along the entire

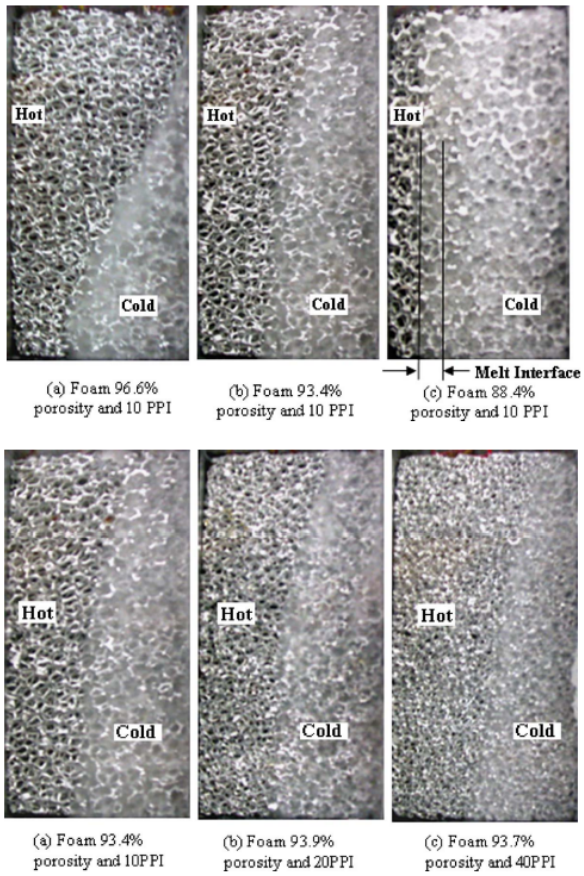

Figure 2.4: Liquid solid interface at time= 80 (bottom) and 75 (top) minutes from applying heat for different pore size aluminium foams(bottom) and different porosity aluminium foam(top) [6]

length of the container. Seemingly this might pose a problem with temperature distribution in PCM leading to a non-uniform distribution across length between the PCM and Thermal Conductivity Enhancer (TCE). This ultimately results in a reduction of the thermal performance of the system. To combat this problem a variable porosity metal matrix was developed. For this effect, a numerical study was performed. It was found that the optimum overall efficiency is obtained at 0.85 porosity although this results in a poor temperature distribution along the length of the system which results in an uneven melting and solidification of the PCM. Based on this, a linear variation of the porosity from 0.95 to 0.85 was used. This approach was able to achieve temperature stabilization at a shorter system length when compared to constant porosity in the metal matrix, the energy efficiency was found to be slightly higher in the variable porosity system. This configuration was also able to achieve a uniform melting process along the system when compared to a constant porosity. A parametric study comparing the effect of the system's length on heat transfer between the PCM and heat transfer fluid (HTF) reveals that length plays a minor role in the process when compared to other variables such as the ratio of shell to tube diameter. Ultimately the conclusion is that a storage volume can be reduced with a variable porosity matrix while still achieving the same thermal performance.

One thing to consider is the limitations of using porous metal matrixes with PCM. The porous metal matrix and the PCM interface can create high thermal resistance, which reduces the rate of heat transfer. Also, the amount of heat that can be stored in such a system is limited by the volume of the matrix and the specific heat capacity of the PCM. Additionally, compatibility between the PCM and the metal matrix must be carefully considered, as some PCM can react with the metal matrix and cause degradation over time. The cost of porous metal matrixes can also be a drawback, especially if the metal used is rare or the manufacturing process is complex. Finally, porous metal matrixes can have poor mechanical stability, which limits their ability to withstand high temperatures, pressures, and thermal cycling. For these reasons, it is important to design a system which takes into consideration its operation conditions, as well as other variables that might impact the system such as materials and geometry.

Production of porous metal matrixes

There are several methods that can be used to produce porous metal matrixes, each with its own advantages and disadvantages. Some of the most commonly used methods are:

- Powder metallurgy - This method involves mixing metal powders with a binder to form a compact, which is then sintered to form a porous structure. The advantages of this method include a relatively low cost, the ability to use a variety of metals, and the ability to produce complex structures. However, there are disadvantages such as limited control over pore size and distribution and difficulty producing highly porous structures. [50]

- Electroforming - This method involves depositing metal onto a template using an electrochemical process. The template can be designed to have a porous structure, which is then transferred to the metal. The advantages of this method include good control over pore size and distribution, high precision, and the ability to produce complex structures. Disadvantages include being limited to metals that can be electrodeposited, being time-consuming, and being expensive. [50]

- Electrospinning - This technique involves electrostatically spinning a metal-polymer composite solution to form a porous fibre mat. The polymer can be removed to leave a porous

metal matrix. The advantages of this method include good control over pore size and distribution and the ability to produce highly porous structures. Disadvantages include being limited to metals that can be electrospun, being time-consuming, and being expensive. [50]

- Foaming - Typically this method introduces a blowing agent into a metal melt, which then expands to form a porous structure. The advantages of this method include good control over pore size and distribution and the ability to produce highly porous structures. Disadvantages include being limited to metals that can be foamed, being expensive, and the foaming agents affecting the metal's properties. [51]

- Addictive manufacturing - Lastly this type of method involves using a 3D printer to build a porous metal matrix layer by layer. Advantages of this method include good control over pore size and distribution, the ability to produce complex structures, and being flexible in terms of metal selection. It is also worth highlighting that disadvantages include being expensive and requiring post-processing to achieve the desired porous structure. [50]

Malaya *et al.* [50] did a review of the different techniques highlighted above and concluded that addictive manufacturing, 3D printing, is identified as a better alternative to the other ones, particularly the selective laser melting route. Addictive manufacturing offers the ability to control not only pore size and distribution but variables such as volume and surface area at will which may pose a breakthrough in the production of metal matrixes. However, further research is needed to optimise the process and improve the properties of the matrixes produced.

2.1.8 Lattice structures

By using metal materials for the matrix and 3D printing, there is also the possibility to create a tailormade structure for each specific use. This allows for a great degree of control over porosity and pore density which, as said before, has been shown to greatly affect heat transfer rate [2]. The resulting structures are called lattices. Recently, the use of a class of periodic cellular structures known as Triply Periodic Minimal Structures (TPMS) in heat transfer applications has received a lot of attention. TPMS structures are minimal surface-based architectures that are mathematically modelled and describe the geometry of repeating patterns in three dimensions [7]. Under both isothermal and isoflux conditions, Qureshi *et al.* [9] compared the heat transfer performance of TPMS lattices to that of conventional metal foams represented by Kelvin cells (Figure 2.5). The applied heat flux was in the 1,000-3,000 W/m2 range. Three TPMS structures were investigated, namely IWP, Gyroid, and Primitive (Figure 2.5) and their heat transfer performance was compared to conventional metal foam. They discovered that all TPMS structures outperformed conventional metal foam in both pure conduction (no buoyancy effects) and with liquid PCM buoyancy.

Catchpole-Smith *et al.* and Qureshi *et al.* [52,53] used the steady state method and an experimental investigation, respectively, to characterize additively manufactured TPMS-based lattices for thermal conductivity. Both discovered that the thermal conductivity of TPMS lattices was determined not only by porosity but also by the architecture of the TPMS lattices. If geometry is of great contribution to thermal efficiency then it must be carefully selected. Qureshi *et al.* [7] conducted a study to this effect, comparing the use of primitive and IWP structures. Although both structures presented similar results the primitive-based system was slightly better at temperature mitigation. Smith *et al.* [54] also compared different types of cell geometry. The

study reports that at the same volume fraction, unit cell types with higher minimum wall thickness have higher thermal conductivity than those with lower minimum wall thickness and also thermal performance for convective heat transfer is typically proportional to the surface area, so thin walls are likely to be more beneficial under convection. Additionally, fluid may flow freely between larger unit cells when compared to smaller ones, increasing the measured thermal conductivity. This effect is more pronounced in unit cell types with a lower surface area to volume ratio, such as the primitive.

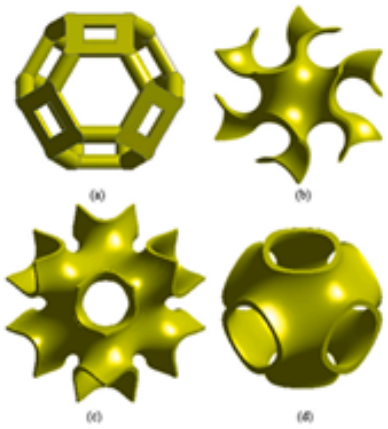

Figure 2.5: TPMS cells: (a) Kelvin, (b) Gyroid, (c) IWP, and (d) Primitive [7].

2.2 Closing remarks

To close this chapter a summary of the presented literature needs to be done. There are a lot of different ways to enhance PCM thermal potential however matrixes and lattices may pose a greater advantage when it comes to thermal conductivity enhancement. Merlin *et al.*1 [55] compared three different methods of thermal conductivity enhancement experimentally: finned exchangers, graphite powder and an Expanded Natural Graphite matrix. The container used consisted of a heat exchanger tube where the outer annular portion is filled with the PCM. When measured, the Overall Heat Transfer Coefficient between the operating fluid and PCM was higher for the configuration using a matrix and measured at around 100 times higher than with the PCM alone.

Considering the geometry of the matrix to use there does not seem to be a consensus on which is ultimately the better alternative. Depending on the choice of PCM this geometry may vary. The choice of PCM, however, typically depends mostly on the operating temperature range but can also greatly vary according to the system characteristics and requirements. Properties and comparison of different PCM can be found in Tables 1.1, 1.2, and in Figure 2.6. Corrosion is also a concern that affects the performance of PCM in various applications, particularly those where the PCM are exposed to harsh environments. Matrices can be particularly susceptible to corrosion due to constant contact with the PCM and heavy thermal cycling, leading to degradation over time. Paraffin waxes, being non-reactive and having a low melting point, are widely used for corrosion protection in metal matrixes. Eutectic alloys, which are mixtures of metals with a lower melting point than the individual metals, are also non-corrosive and can prevent corrosion. PCM based on salts, such as calcium chloride or sodium acetate, have low vapour

pressure and are non-reactive, making them suitable for use in metal matrixes to prevent corrosion. Nanoparticle PCM, made from materials like ceramics, are non-corrosive and have high thermal stability and low thermal conductivity, making them ideal for use in metal matrixes. [8]

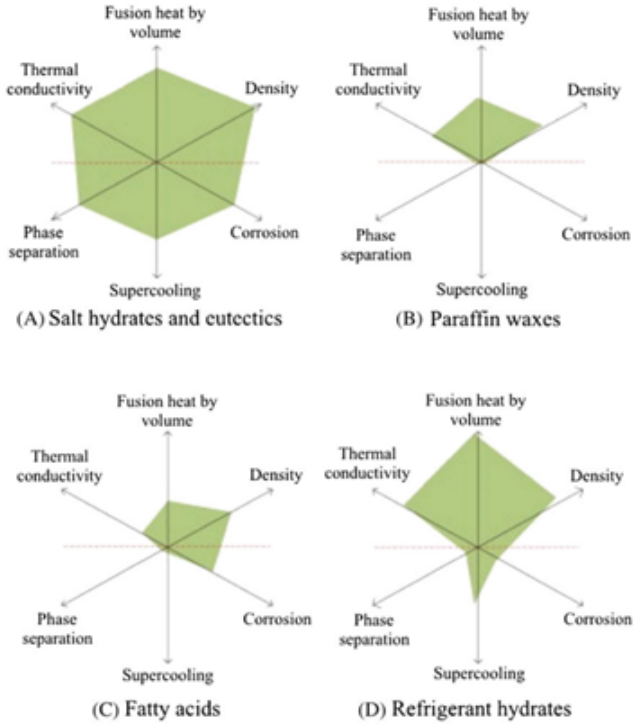

Figure 2.6: Thermal properties of various PCM [8].

It is also important to recollect the findings of Kumar and Saha [6] which showed that a high porosity matrix performs thermally better than a lower porosity matrix due to the aid of convection. This would of course be nullified in a system where the PCM possesses a high viscosity value, making the contribution of convection very low when compared to conduction. A higher porosity matrix also allows for a larger amount of energy stored when compared with lower porosity. This is because of the bigger volume of PCM that the system can hold. The more PCM the system holds, the higher the thermal capacity becomes. There might be an ideal value between the volume of PCM and metal material in the system however. Thus lattice and TPMS use with PCM proves to be a relevant topic of investigation.

2.3 Study's main objective

Moving forward the primary goals are:

- To use and validate a methodology for simulating a matrix plus PCM system,
- Employ the methodology to investigate the system's thermal performance and identify ways to enhance its efficiency through parameter manipulation.

Achieving these goals will involve creating a computational model of a matrix plus PCM system and validating it. The simulation will entail analyzing the heat storage process occurring

in the system. This translates to analysing the liquid fraction of the PCM, which is the volume fraction that has been converted from solid to liquid, and the convergence rate which represents how fast liquid fraction and heat storage are achieved. Once the methodology has been defined and tested, the properties of the system will then be varied to verify how they influence its performance.

The ultimate goal of this dissertation is to draw conclusions regarding the best design and configuration of matrix plus PCM systems for various applications. The results obtained can be used to optimize the thermal performance of thermal energy storage systems, leading to increased energy efficiency, reduced environmental impact, and lower operational costs.

In conclusion, this dissertation aims to create a methodology for simulating matrix plus PCM systems, investigate the impact of varying its properties, and draw conclusions regarding the optimal configuration for different applications. This study is significant as it will provide insight into the design and performance of thermal energy storage systems, leading to more efficient and sustainable energy usage.

Chapter 3

Methodology and model validation

3.1 Methodology

After conducting an extensive literature analysis, our subsequent course of action involves modeling and testing a porous metallic structure filled with the selected PCM. In order to simulate the behavior of the PCM under energy transfers, a paper by Q. Zahid Ahmed *et al.* from 2021 was used as a reference for calibrating the Computational Fluid Dynamics (CFD) numerical model [9]. Although the primary focus of the aforementioned article is to compare TPMS structures with naturally-formed porous structures, it can be adapted to our specific problem. The article supplies all the essential information required to model the geometry, establish material parameters, and define simulation setups, which can serve as a valuable starting point for our own endeavors. As an initial approach, we will commence by modeling the Kelvin-cell based structure employed in the cited article and subsequently extend our analysis to other structures.

Initially, the structure to analyze needs to be considered. It can be represented as a porous structure using the model shown in Figure 3.1. However, due to symmetry, a simplified model, also illustrated in Figure 3.1, is better suited to save computing time and resources. The simplified model represents one of the many columns of the original model and takes advantage of the fact that there is symmetry between these collumns.

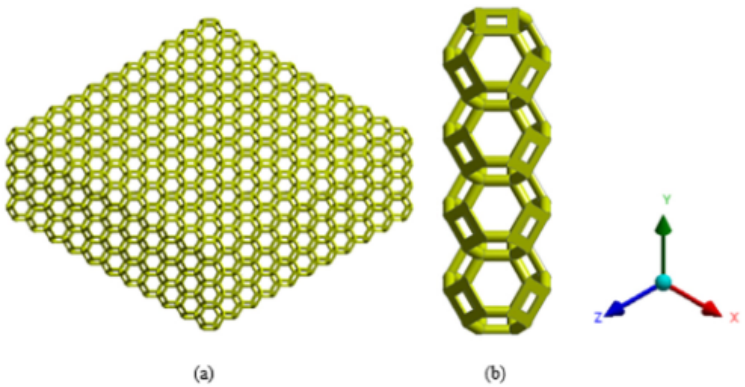

Figure 3.1: (a) Model of porous structure , and (b) Simplified geometry [9].

This design was created using nTopology software, specifically the nTop tool. This software specializes in CAD body creation through implicit modeling, where the mathematical represen-

tation of a solid object is encapsulated in a single equation, allowing for faster design processes and simplified development of complex structures [56].

Using nTop, a box-like body was created and converted into a porous lattice with the desired geometry. The geometry can be adjusted through various parameters such as cell size, in which the box itself that contains the matrix can be altered, box size, in which x, y and z dimensions can be altered, cell thickness and cell type. The shape to be replicated can be selected from a wide range of choices, from simple cubic to diamond.

nTop allows for the creation of multiple configurations of porous matrices, which were then easily transferred to the chosen CFD software, Ansys®. In order to export the bodies with all their properties recognized, a .STL format was utilized. The process involved applying a voxel grid and surface meshing to the lattice plus PCM structure to retain all details. Subsequently, a split mesh operation was performed to eliminate any duplicated or imperfect meshes that could create problems in creating a volumetric mesh. Finally, a re-meshing step was executed to ensure that there were no geometry issues such as self-intersecting surfaces. Following this process, the bodies are ready for exportation. A visual representation of the entire process until exportation is presented in the flowchart depicted in Figure 3.2.

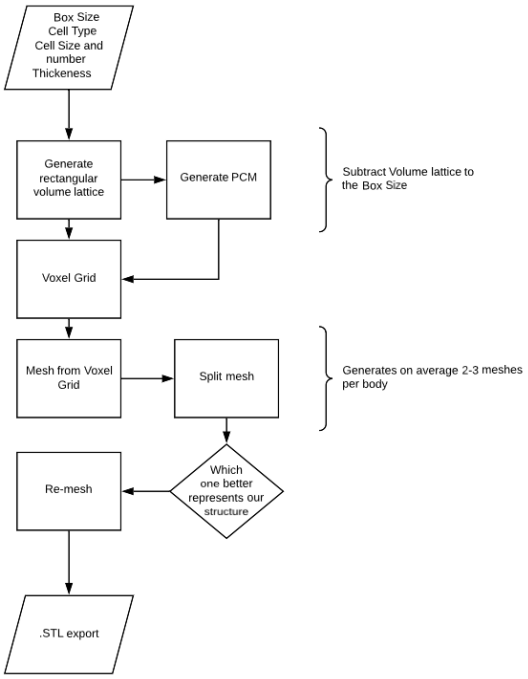

Figure 3.2: Flowchart of structure creation process

The .STL format is then imported into Ansys® for further analysis. Upon importing the bodies, boundary conditions are defined using SpaceClaim so that the system's conditions can be replicated in the simulation environment. Moving on to the mesh creation process, Fluent meshing is utilized to refine mesh parameters and generate a mesh with appropriate accuracy. Since the imported files have already undergone surface mesh treatment, the wrap parameter is utilized instead of the typical surface mesh to prevent loss or overlap of detail created in nTop. After generating the surface mesh, a volumetric mesh is required to consider the inside of the structure in the analysis. Before proceeding with the simulation setup and solution, it is essential

to assess whether this is the best setup for the experiment. A mesh optimization was attempted but it quickly became evident that adding detail to our mesh would only strain the system and condition the results. Since the goal is not to build the ideal simulation model but instead a replicable model which allows for variation comparison, a simplified mesh suffices.

In preparation for the simulation, the model is simplified by making the following assumptions,

- The fluid flow is assumed to be Newtonian, incompressible, and laminar,
- The impact of gravity was accounted in the y-axis,
- The Boussinesq approximation is used to simulate the effects of buoyancy,
- The sharp melting interface is represented by a mushy zone, where the PCM was neither solid nor liquid but a mixture of both.

The next step involves setting up the simulation. The governing equations are solved using double precision on a 15-core CPU, and a pressure-based finite volume approach is used to discretize the equations. An enthalpy-porosity model, as described in ANSYS Fluent User Guide, is used for this phase change simulation. Initially, a segregated solver with a PISO approach was used for pressure-velocity coupling, but it was found to consume too much computing power and time, so a SIMPLE approach was used instead. The convective terms of the governing equations are discretized using a second-order upwind technique, and the pressure-velocity coupling is performed using the PRESTO algorithm. Residuals are set to 10^{-4}, 10^{-5}, and 10^{-9} for the continuity, momentum, and energy equations, respectively. The simulation is performed with a time step of 1 second and 40 iteration timesteps, due to not having access to a large amount of computing power and the need to run several simulations. An overview of the Ansys® process can be seen in Figure 3.3. The model is ready to be tested.

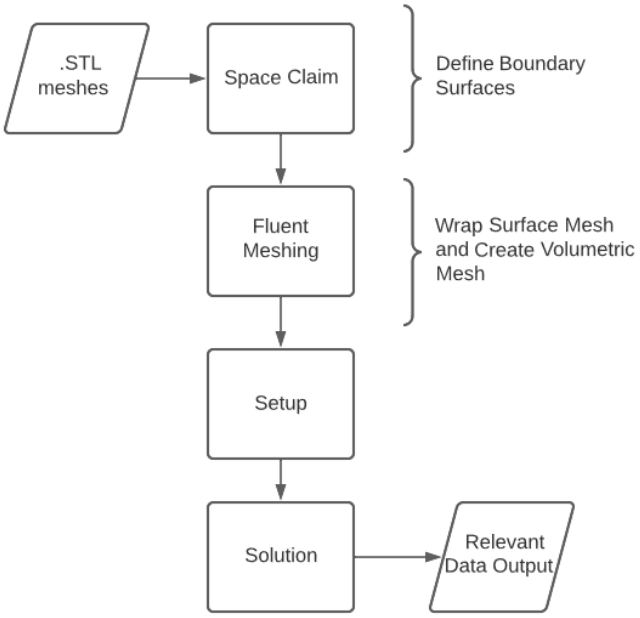

Figure 3.3: Flowchart of Ansys® methodology

3.2 KPIs

In order to evaluate and compare the results, a set of Key Performance Indicators (KPIs) is required. Typically, liquid fraction over time is an accurate indicator of how well the model is doing, as in [9]. Achieving a higher liquid fraction faster would indicate a preferable structure, but this is true only if the volume of both the lattice and PCM remains unchanged during comparison or the so-called porosity. However, if the configuration is changed to test out how different parameters might influence performance and compare different structures, which ultimately varies porosity, using liquid fraction over time may be a bit more challenging. Since the structures' volume stays the same across all configurations, 1372 mm^3, it is possible to normalize the liquid volume at each timestep of the simulation by using the following expression:

$$KPI_1 = \frac{liq_f \times V_P}{V_t} \quad [-] \tag{3.1}$$

where liq_f represents the liquid fraction over time, V_P represents the total PCM volume for each configuration, and V_t represents the total volume of the structure. By using this metric, it is possible to make comparisons across all configurations even though porosity is not the same. By plotting the value of KPI_1 over time amongst different configurations the maximum value for this KPI will appear different for different structure configurations. This is to be expected as it represents the different porosity of each system. A higher value for KPI_1 at a given timestep indicates a better performance for a given structure as it translates to a higher value of PCM that has changed phases from solid to liquid.

The next and final KPI is the heat stored over time. This can be determined by calculating the heat flux through the bottom heated surface per timestep and applying an integral so that the amount of heat stored until a specific time can be calculated.

$$KPI_2 = \int_0^t \int_A q'' dA dt \quad [kJ] \tag{3.2}$$

This KPI is particularly useful since it is a direct correlation with the application intended for these systems, which is a Thermal Energy Storage system. A higher value of KPI_2 would also mean a better structure configuration. The given unit for KPI_2 is in $kiloJoule$ (kJ).

Moving forward, KPI_1, KPI_2 and also convergence rate will be used to compare different cases. The KPIs have been defined above, but convergence refers to the rate at which the specific configuration being analyzed, for instance the reference simulation for Kelvin-based structures, converges to its maximum value of KPI_1 or KPI_2.

3.3 Case study for model validation

For this case study the chosen PCM was Parafine Wax. This PCM was selected due to the properties mentioned in section 2.2 and it's wide use with metal lattices as seen in the literature review (2).

The simplified model for the system comprises a vertical cell arrangement of Kelvin-type cells with 7-*mm*-sized cells. The total height of the cell arrangement corresponds to four stacked cells, i.e., 28*mm*. The lattice and PCM volumes were established by maintaining a porosity of approximately 90%, following literature recommendations. This indicates that the PCM occupies 90% of the total system volume, which is reflected in the lattice's thickness set to 0.930 *mm*.

In accordance with Figure 3.1, the structure size is 7 $mm \times 7\ mm \times 28\ mm$, with a cell size of 7 $mm \times 7\ mm \times 7\ mm$ for the specified cell type. Following the definition of the structure, a voxel grid was implemented with a voxel size of 0.05 mm. Subsequently, voxel meshing and mesh splitting were performed, and a remeshing process was conducted with an edge length of 0.5 mm to ensure an accurate representation of the structural details using triangle-shaped elements. A full overview of the system input parameters can be seen in figure 3.4a and 3.4b.

The final body export can be seen in Figure 3.5.

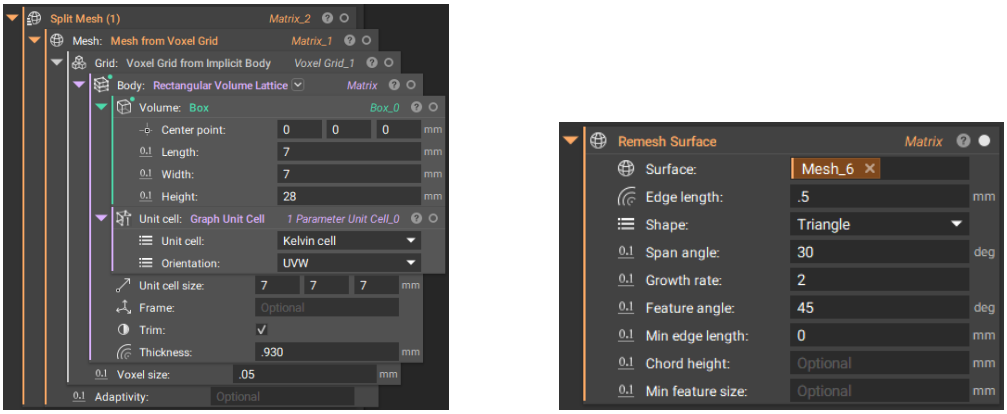

(a) (b)

Figure 3.4: (a) Split mesh, voxel grid, and body creation (b) Remesh surface operation

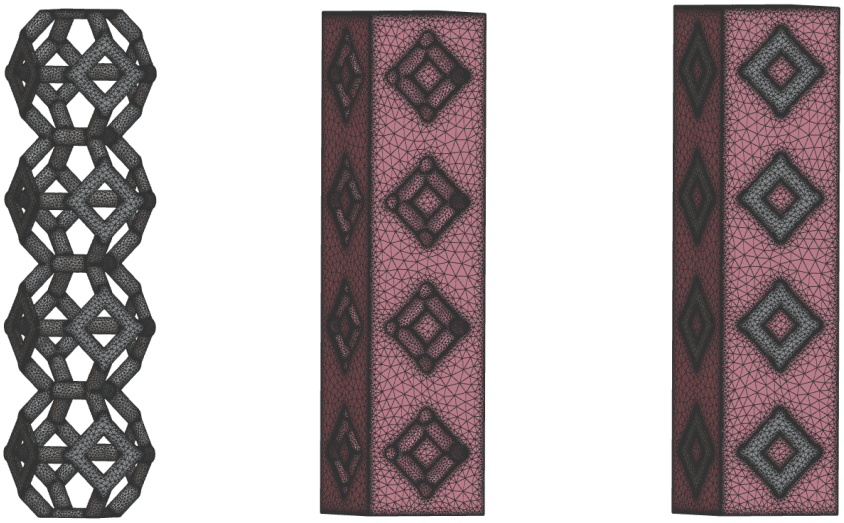

(a) (b) (c)

Figure 3.5: (a) .STL mesh of metal matrix (b) .STL mesh of PCM (c) both meshes joined

After importing the model into Ansys®, the boundary conditions are established as depicted in Fig. 3.6. In this particular scenario, the structure experiences a uniform bottom heat at 344 K, contrasting with its initial setup temperature of 300 K. To reproduce the observed pattern illustrated in Figure 3.1, a lateral symmetry boundary condition is implemented. On the top surface,

an adiabatic boundary condition is enforced to hinder any heat transfer through it. Furthermore, a boundary condition representing the interface between the interior of the PCM and the metal matrix is defined which acts as a conjugate heat transfer interface.

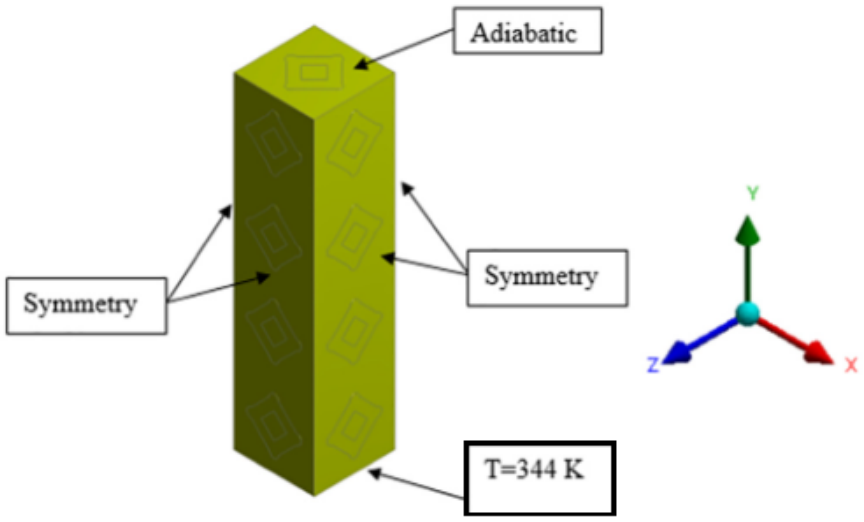

Figure 3.6: Simplified model with boundary condtions [9].

During the mesh generation process, the surface mesh is created with local sizing mesh elements ranging from 0.7 mm to 0.023 mm for curvature and 0.013 mm for proximity. In the volumetric stage, 3 inflation layers are applied with a growth rate of 1.2, resulting in a mesh characterized by an orthogonal quality of 0.70, a skewness of 0.29, and a total of 445,000 cells. While these values may appear relatively low according to quality standards, they are to be expected given the problem's nature and the high curvature of the elements. As mentioned, further refining the mesh would significantly slow down simulations and impact the rate at which results could be obtained. Despite this, mesh optimization was attempted but it quickly became a burden on the system and did not consistently produce results due to the mesh's high level of detail. Therefore, this mesh configuration is believed to capture enough detail to produce valid results.

The material properties for the paraffin PCM (RT-42 from Rubitherm [57])[1] and the specific type of aluminum employed in the simulation are provided in Table 3.1. T_s and T_l represent the temperatures for the beginning and end of the mushy zone, respectively, for the PCM.

It is worth mentioning that the default aluminum material in the software was used for the simulation, which may differ slightly from the material specified in the referenced article. Nevertheless, this discrepancy does not compromise the setup's validity or the accuracy of the simulation results; it merely influences the heat transfer process due to variations in material properties.

[1] https://www.rubitherm.eu/en/productcategory/organische-pcm-rt

Table 3.1: Thermophysical properties of the materials

Material	$\rho(kg/m3)$	c_p (J/ kg.K)	k (W/ m.K)	$\beta(1/K)$	L (J/kg)	T_s (K)	T_l (K)	$\eta(kg/m.s)$
PCM	880	2000	0.2	0.0001	165000	311.15	316.15	0.0235
Aluminum	2719	871	202.4	-	-	-	-	-

3.3.1 Case study results

The simulation results are presented in Figure 3.7. As expected, the total liquid fraction is reached and at around 300 seconds. There are some differences, however, when compared with the referenced article [9]. In their study, Q. Zahid Ahmed *et al.* achieved a total liquid fraction at around 400 seconds, which could be attributed to the use of a different type of aluminum for the metal matrix, a different mesh refinement, and the influence of using different solution methods and timesteps. Additionally, there may be slight variations in the characterization of boundary conditions. Despite these differences, our model provides a reasonable simplification of the referenced study, which is sufficient for comparing different parameters.

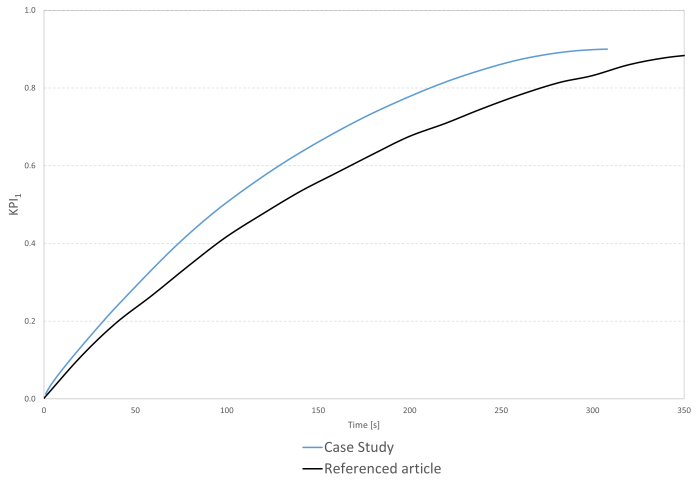

Figure 3.7: KPI_1 comparison between this document's case study and the referenced article

Intentionally blank page.

Chapter 4

Parameter setting and configuration

4.1 Strategy outline

After calibrating the simulation model and devising ways to evaluate the performance of the several cases simulated, the next step is to identify the parameters that affect our structure. In order to do this a parametrization is done under three categories:

- Cell type variation between three different types,
- Cell size variation to double and half the initial value and
- Thickness variation to double and half the initial value;

It should be noted that the methodology for the parametrization simulations was slightly modified due to the PRESTO algorithm causing errors when the parameters were changed. This is not uncommon as the mesh requirements and simulation setup can vary depending on the specific problem being analyzed. To mitigate these errors, the decision was made to switch from the PRESTO to the SIMPLE algorithm. To ensure that this change did not impact the solution, the calibration simulation was re-run and the results were compared. Upon overlapping the two curves obtained, there were no discernible differences. Additionally, when calculating the error for each time step, it was found to be less than 0.25%, with a maximum error of 0.22%. These findings suggest that the switch in algorithms does not significantly impact the solution and allows us to proceed with confidence.

It is also important to mention that when halving the thickness of the Gyroid structure, the material thickness of the matrix becomes significantly reduced, posing a challenge for Ansys® to convert it into a volumetric matrix. Consequently, results could not be obtained for this particular case. To ensure comparability across different cell types, no further reduction in thickness was attempted.

4.2 Parameter configuration

4.2.1 Cell type

Initially, simulations were run to observe how a different lattice design would perform under the same conditions as the calibrated simulation model. This was achieved by running simulations for two more lattice types: an IsoTruss cell-based lattice and a Gyroid cell-based lattice, as seen on Figure 4.1. These designs were evaluated using the methodology described earlier. The

Gyroid-type lattice falls under the TPMS category, as mentioned in our literature review. The goal was to determine the impact of a different lattice design on the heat transfer rate of the structure, similar to the approach taken by Q. Zahid Ahmed *et al.* in their article. The mesh structures for both lattice designs can be seen in Figure 4.1.

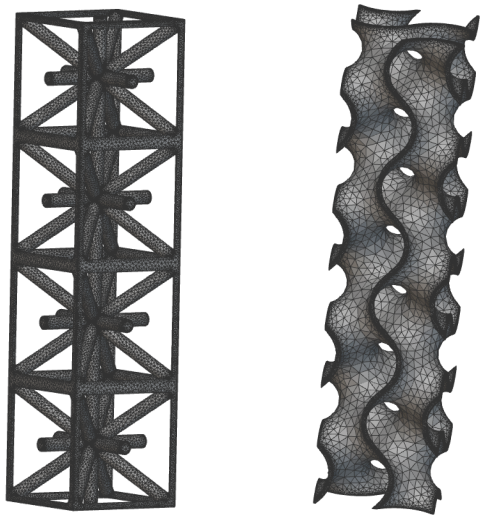

(a) (b)

Figure 4.1: (a) .STL mesh of IsoTruss-type lattice (b) .STL mesh of Gyroid TPMS lattice

4.2.2 Cell size and thickness

The impact of cell type on heat transfer rate is one aspect to consider, but what about other parameters? It's possible that varying the initial configuration for each cell design could enhance the system's performance. As depicted in our flowchart in Figure 3.2, parameters such as cell size and thickness can be altered during the creation of our lattice, and such modifications might offer a significant advantage. To test this hypothesis, we focused on a parametrization of these two variables. Initially, we changed the height parameter of the cells from 7 mm to 14 mm and 3.5 mm, resulting in a decrease and increase in the number of cells for each structure, respectively. We refer to the 3.5 mm case as a doubling of the cells and the 14 mm case as a halving of the cells for convenience. The properties for these configurations are listed in Tables 4.1, 4.2, and 4.3.

Then the thickness of the lattice was varied to double and half the amount of the reference simulation for each cell type. For the Kelvin-type cell, the reference thickness was 0.930 mm, for the IsoTruss-type cell, it was 0.780 mm, and for the Gyroid TPMS cell, it was 0.350 mm. The properties for these configurations are also shown in Tables 4.1, 4.3, and 4.2. However, a limitation was encountered in the simulation model where the case of halving the thickness for the Gyroid structure could not be handled due to difficulties in defining a volumetric mesh. As a consequence, the results for this case could not be analyzed. Also, as will be pointed out in future chapters, by reducing the thickness of the geometry, the number of timesteps to complete the simulation increases in a great extent. So that this simulation can be analyzed the timesteps were increased from 400 to 1500 for the cases with thickness reduction. Due to this change, the x-axis of graphs representing cases with half the amount of thickness need to be adjusted to a

logarithmic scale in order to accommodate every detail in a readable form.

Table 4.1: Volume and surface area for Kelvin-type structures

Geometry	Volume of PCM(mm^3)	Surface Area(mm^2)	Thickness(mm)
Kelvin ref	1234.80	1106.84	0.930
Half Cells	1274.74	1221.42	0.930
Double Cells	1150.17	1451.12	0.930
Double Thickness	922.74	1263.44	1.860
Half Thickness	1335.21	1089.00	0.465

Table 4.2: Volume and surface area for IsoTruss-type structures

Geometry	Volume of PCM(mm^3)	Surface Area(mm^2)	Thickness(mm)
IsoTruss ref	1225.87	1368.04	0.780
HalfCells	1268.00	1268.40	0.780
Double Cells	1133.24	1682.80	0.780
Double Thickness	875.00	1512.00	1.560
Half Thickness	1332.95	1161.73	0.390

Table 4.3: Volume and surface area for Gyroid-type structures

Geometry	Volume of PCM(mm^3)	Surface Area(mm^2)	Thickness(mm)
Gyroid ref	1237.44	1261.07	0.350
Half Cells	1263.00	1081.66	0.350
Double Cells	1202.6	1744.41	0.350
Double Thickness	1103.00	1324.00	0.700
Half Thickness	1304.00	1238.00	0.175

Intentionally blank page.

Chapter 5

Parametric Study

5.1 Cell Type variation

The system's performance appears to be affected by the type of cell used, specifically the Kelvin, IsoTruss, and Gyroid structures. This can be observed in Figures 5.1 and 5.2, where three distinct curves for KPI_1 and KPI_2 over time are noticeable, despite the only difference between configurations being the cell type. The three curves converge to a value of 0.9, representing 90% porosity.

In terms of KPI_1, the IsoTruss structure slightly improves upon the results of the Kelvin structure by a constant margin of 3%, reaching maximum KPI_1 approximately 10% faster. The Gyroid structure, however, converges significantly faster to its maximum value of KPI_1, achieving it 33% faster or in 100 seconds less.The time to reach maximum KPI_1 or total liquid fraction was 305 seconds for Kelvin, 268 seconds for IsoTruss, and 205 seconds for Gyroid.

Similarly, for KPI_2, the Gyroid structure outperforms the other two, while the IsoTruss outperforms the Kelvin structure. Maximum KPI_2 is approximately the same for the three configurations due to their relationship with porosity, which is consistent at around 90%.

Figures 5.3, 5.4, and 5.5 depict the liquid fraction over time. These Figures have been inverted through the y-axis, observable in Figure 3.6, to allow for more effective visualization of the liquid fractions they represent. By analyzing these results it is clear that the gyroid structure outperforms the other structures.

The variances between structures are unsurprising since the Kelvin-based structure was created to mimic the formation of natural metal foam, while the IsoTruss and Gyroid structures were intentionally engineered to enhance heat transfer performance.

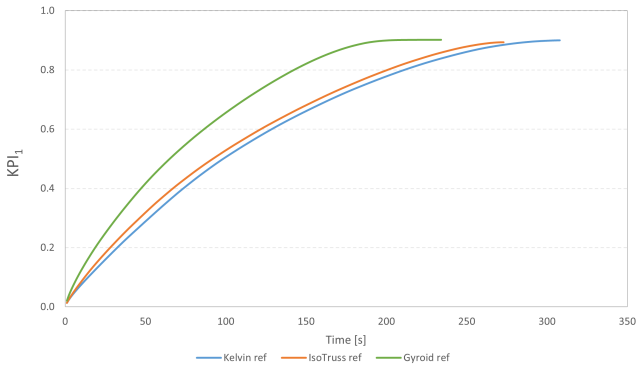

Figure 5.1: KPI_1 comparison between Kelvin, IsoTruss and Gyroid

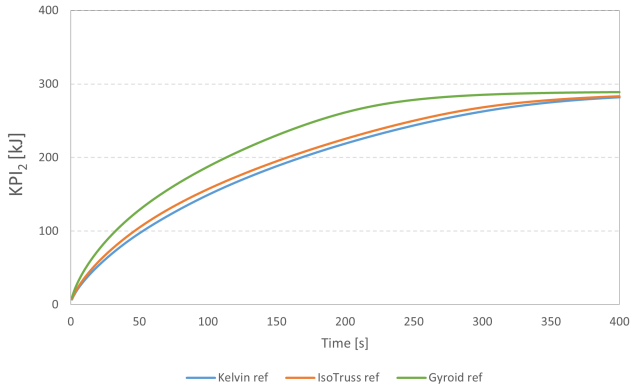

Figure 5.2: KPI_2 comparison between Kelvin, IsoTruss and Gyroid

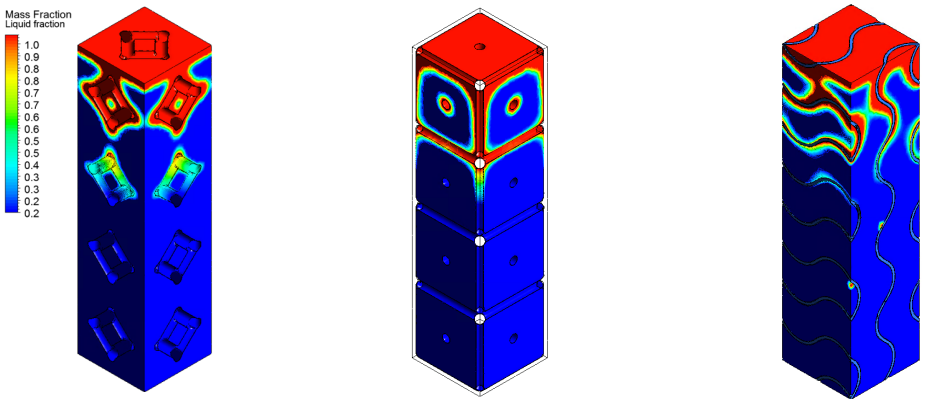

(a) (b) (c)

Figure 5.3: PCM liquid fraction at 10s for the $7mm$x$7mm$x$28mm$ structure of (a) Kelvin reference case (b) IsoTruss reference case (c) Gyroid reference case

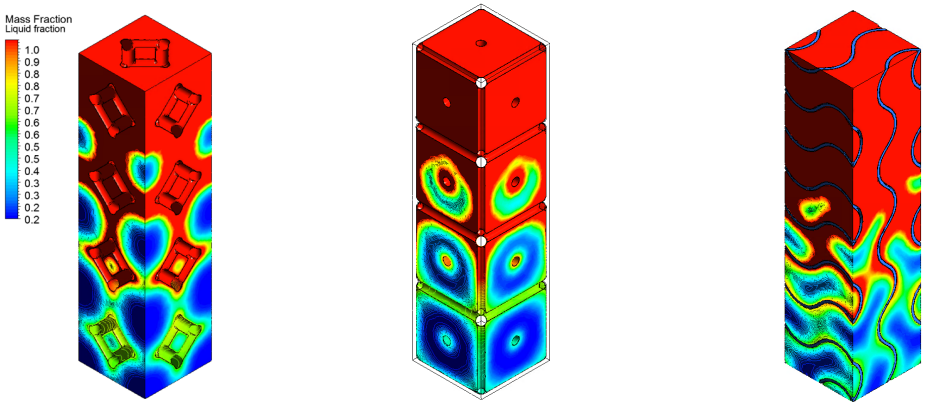

(a) (b) (c)

Figure 5.4: PCM liquid fraction at 100s for the $7mm$x$7mm$x$28mm$ structure of (a) Kelvin reference case (b) IsoTruss reference case (c) Gyroid reference case

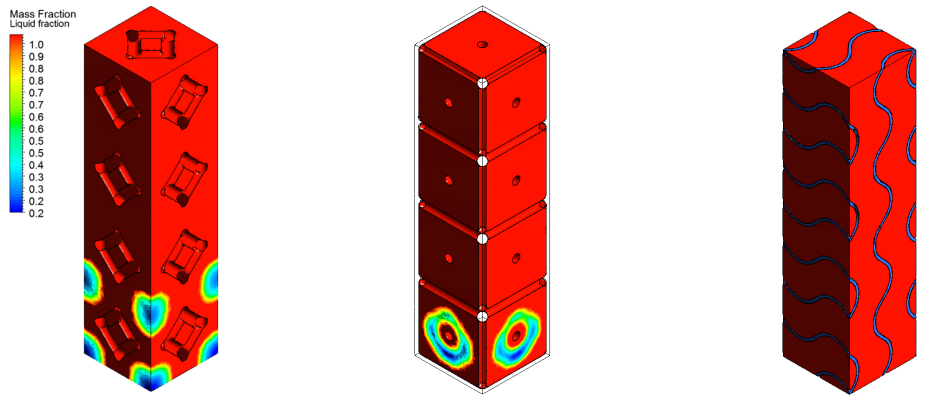

(a) (b) (c)

Figure 5.5: PCM liquid fraction at 250s for the $7mm$x$7mm$x$28mm$ structure of (a) Kelvin reference case (b) IsoTruss reference case and 220s for (c) Gyroid reference case

5.2 Cell size variation

With this parametric study, the intent was to observe if increasing or decreasing the number of cells for each configuration would yield different results. By varying cell size the direct result is a modification to the number of cells. This also slighlty affects the systems properties such as porosity and surface area. A property comparison can be viewed in Tables 4.1, 4.2 and 4.3 and values for KPI_1 and KPI_2 over time are available at Figures 5.6, 5.8 and 5.10 for KPI_1 and 5.7, 5.9 and 5.11 for KPI_2.

A liquid fraction visualization for cell size variation can be found in Figures A.1, A.2, A.3, A.4, A.5, A.6, A.7, A.8 and A.9.

5.2.1 Decreasing cell size

By reducing the cell size from 7 mm to 3.5 mm, the number of cells within each matrix is doubled. Consequently, the cell count increases from 4 to 8 within the same structure. This results in a decrease in the volume of phase change material (PCM) contained in the structure, while simultaneously increasing the surface area of the matrix. The degree of change varies across different structures. The doubling of cell quantity leads to a volume reduction of 7%, 3%, and 8%, and a surface area increase of 31%, 38%, and 23% for the Kelvin, IsoTruss, and Gyroid structures, respectively. It is interesting to see how a higher reduction in PCM volume does not translate to a higher increase in surface area. In fact, these properties appear to show no obvious link.

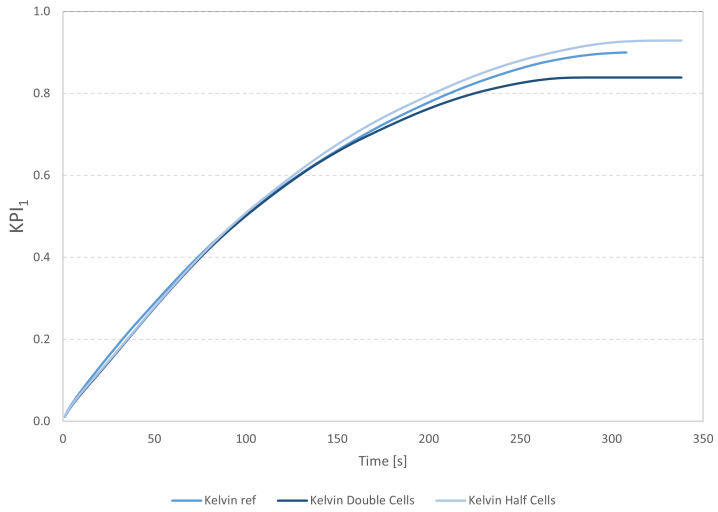

Figure 5.6: KPI_1 comparison between Kelvin reference, Kelvin with double cells and Kelvin with half cells

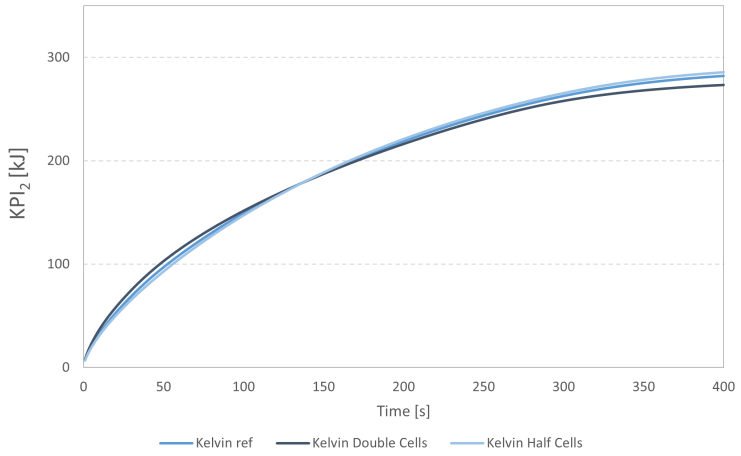

Figure 5.7: KPI_2 comparison between Kelvin reference, Kelvin with double cells and Kelvin with half cells

In regard to the Kelvin structure, the curve between the reference case and the double cell case remains identical. However, the double cell case achieves its maximum value for KPI_1 slightly faster, at around 257 s compared to the reference case's 305 s, resulting in an 18% difference. A similar trend is observed for KPI_2, with the plotted curve being virtually identical, except for a slight difference towards the end. The double cell case also exhibits a lower maximum value for KPI_2, with a 4% difference. This discrepancies can largely be attributed to the lower porosity, as mentioned earlier and evident from the lower maximum value in Figure 5.6.In summary, there is a 4% difference in stored energy for an 18% increase in performance (48 s).

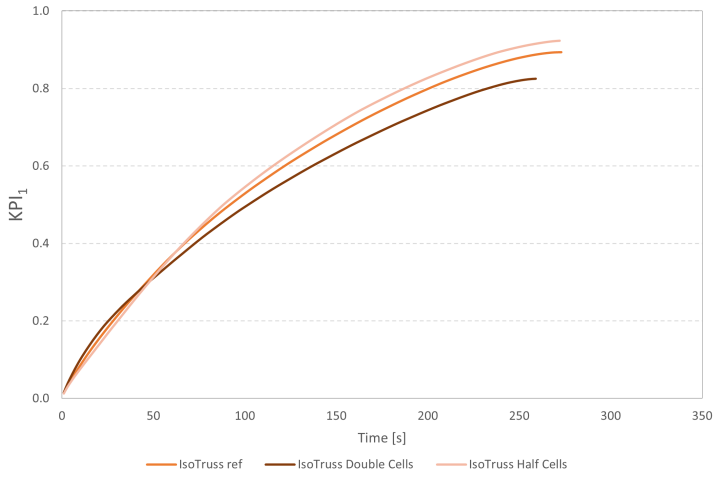

Figure 5.8: KPI_1 comparison between IsoTruss reference, IsoTruss with double cells and IsoTruss with half cells

Turning to the IsoTruss structure, more noticeable differences can be observed for both $KPIs$. Differences in curvature are evident across the entire timeline in Figure 5.8. The double cell case initially outperforms the reference case until the 50 s mark. However, beyond this point,

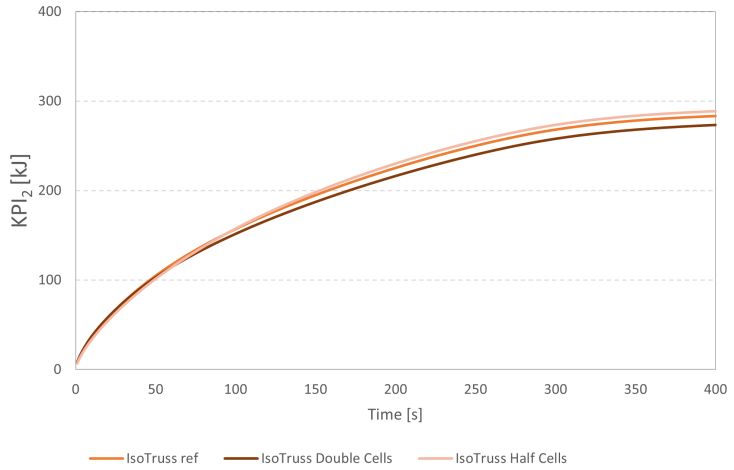

Figure 5.9: KPI_2 comparison between IsoTruss reference, IsoTruss with double cells and IsoTruss with half cells

the reference case consistently exhibits higher values of KPI_1 for each time value. Similar to the Kelvin structure, the double cell case reaches its maximum KPI_1 value faster. The convergence rate difference is 6% or 15 s less for the double cell curve. Regarding KPI_2, the same pattern emerges, with a performance swap occurring at the 50 s mark. Similar to the Kelvin configuration, the double cell case achieves a lower maximum value of KPI_2, with a 3% difference compared to the reference case. To summarize, there is a 6% increase in the convergence rate related to liquid fraction and a 3% reduction in stored energy capacity.

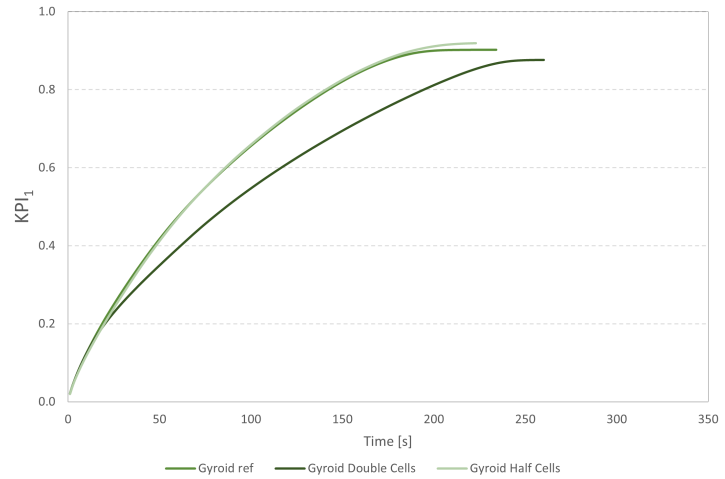

Figure 5.10: KPI_1 comparison between Gyroid reference, Gyroid with double cells and Gyroid with half cells

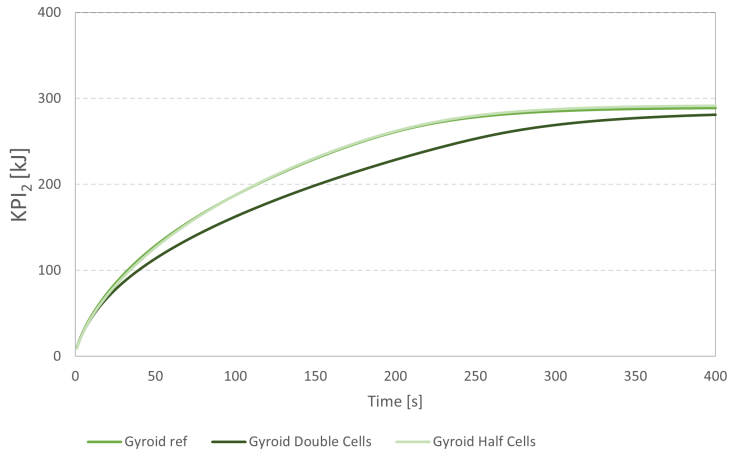

Figure 5.11: KPI_2 comparison between Gyroid reference, Gyroid with double cells and Gyroid with half cells

Lastly, concerning the Gyroid structure, a more significant difference is observed when increasing the number of cells. The curvature for KPI_1 remains indistinguishable until the 25 s mark, from which point onward, the double cell case exhibits significantly poorer performance compared to the reference case. Furthermore, contrary to the earlier described structures, the Gyroid with a double cell configuration reaches its maximum KPI_1 value after the reference case, with a 14% slower convergence rate. This deviation from the expected pattern among these configurations is noteworthy. Similarly, the total value of KPI_1 is lower for the double cell case. In terms of KPI_2, the graph aligns with the pattern observed in previous structures, as the double cell case converges to a smaller value, resulting in a 3% reduction in heat storage capacity. Thus, the Gyroid structure exhibits a 14% performance decrease and a 3% reduction in heat storage capacity when the cell size is reduced.

In summary, reducing the cell size resulted in changes in the properties of the metal lattice structures. The Kelvin structure demonstrated improved performance and faster convergence for both KPI1 and KPI2, albeit with the loss of heat storage capacity (maximum KPI_2). The IsoTruss structure initially benefited from the double cell configuration but eventually presented lower values of KPI_1 for the same timestep eventually converging faster to a lower value. The Gyroid structure deviated from the expected pattern, exhibiting poorer performance and slower convergence with the double cell case.

5.2.2 Increasing cell size

In contrast to the previous effect, increasing the cell size leads to a reduction in the number of cells within the matrix. By halving the cell size, the cell count changes from 4 to 2, resulting in notable changes in the structure's properties. For the Kelvin, IsoTruss, and Gyroid structures, an increase in PCM volume of 3%, 3%, and 2%, respectively, is reported, while a decrease in surface area of 10%, 8%, and 15% can be observed.

Let's begin with the Kelvin structure. Similar to the decrease in cell size, the curvature of KPI_1 remains similar until around the 100 s mark. However, from that point onward, there is a slight increase in KPI_1 per unit of time compared to the reference case, amounting to approximately 2% higher values. The maximum KPI_1 is reached 5% faster as well. The pattern continues with KPI_2, where the half cell case achieves a 1% higher value. This corresponds to an overall increase of 2% in performance and a 1% improvement in heat storage capacity.

IsoTruss exhibits a similar result to the Kelvin configuration. Starting around the 60 s mark, the half cell case slightly outperforms the reference case, with a 4% higher KPI_1 value at each timestep. The time taken to reach the maximum value of KPI_1 is similar for both cases, with no significant variance reported. KPI_2 also shows an increase of 1.7% for the half cell case starting at the 60 s mark.

The Gyroid structure presents an interesting scenario. The plot for KPI_1 of the half cell and reference cases shows two nearly overlapping curves. Surprisingly, varying this parameter for the Gyroid structure causes an impact of less than 0.5% in the KPI_1 values. The half cell case seems to converge at the same rate as the reference case. However, after reaching the maximum KPI_1 value in the reference simulation, the half cell case continues to converge to a higher value. In terms of KPI_2, the difference is also barely noticeable, as the convergence rate for this metric is identical for both cases, resulting in a 0.7% higher value for the half cell case.

Overall, these findings indicate that reducing the cell size in metal lattice structures can enhance their performance and heat storage capacity, but the extent of improvement varies depending on the specific lattice configuration. The Kelvin and IsoTruss structures showed notable enhancements, while the Gyroid structure exhibited minimal changes.

5.3 Thickness variation

The aim of this parametrization was to investigate the impact of varying the thickness of each structure on the results and performance. Altering the thickness leads to changes in porosity and surface area, similar to the variations observed in cell size. Tables 4.1, 4.2, and 4.3 provide a comparison of the properties, while Figures 5.12, 5.14, and 5.16 present the values of KPI_1 over time. Figures 5.13, 5.15, and 5.17 depict the values of KPI_2. Upon initial observation, it is evident that the differences resulting from thickness variation are substantial when compared to cell size.

A liquid fraction visualization for thickness variation can be found in Figures A.10, A.11, A.12, A.13, A.14, A.15, A.16, A.17 and A.18.

5.3.1 Increasing Thickness

By increasing the thickness, the Kelvin, IsoTruss, and Gyroid structures have new values of 1.860 mm, 1.560 mm, and 0.700 mm, respectively. This change in thickness leads to alterations in the properties of each structure. Specifically, the PCM volume decreases by 26%, 29%, and

11%, while the surface area increases by 14%, 10%, and 5% for the Kelvin, IsoTruss, and Gyroid structures, respectively. The impact of thickness variation is more pronounced in the Kelvin and IsoTruss structures, which can be attributed to their larger initial thickness values.

In the Kelvin structure, the curvature of KPI_1 shows significant changes compared to the reference case. The convergence rate is approximately 73% faster, resulting in a decrease of 220 s. This represents a tremendous increase in performance, but it comes with certain drawbacks. The maximum value of KPI_1 for the double thickness case is significantly lower, around 26% less than the reference case. Similarly, the maximum value of KPI_2 is lower, indicating a loss of 11% in heat storage capacity.

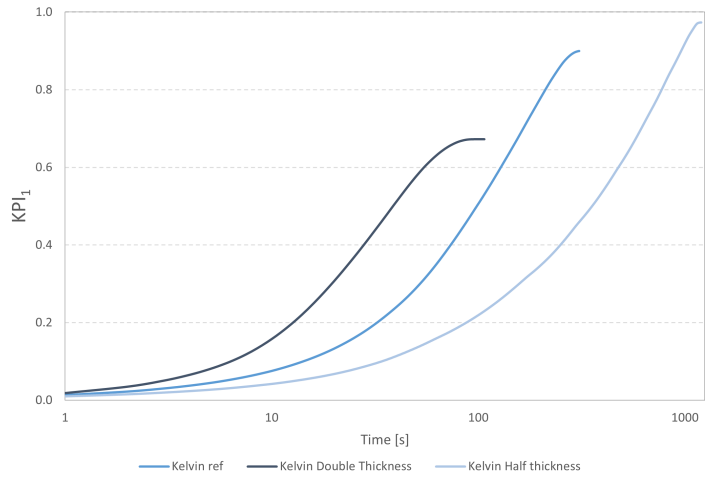

Figure 5.12: KPI_1 comparison between Kelvin reference, Kelvin with double thickness and Kelvin with half thickness

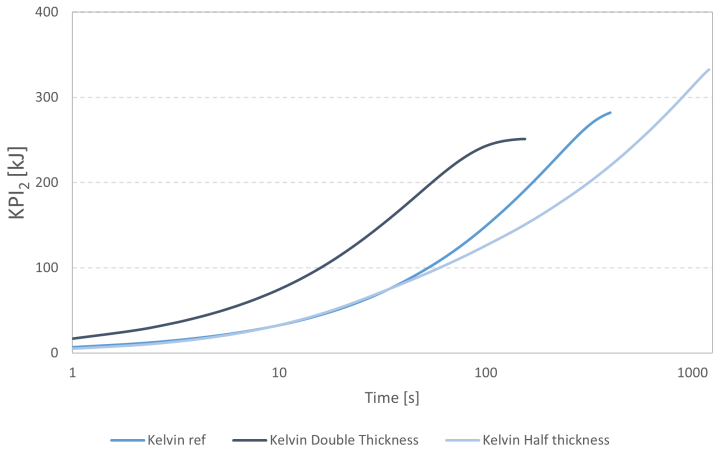

Figure 5.13: KPI_2 comparison between Kelvin reference, Kelvin with double thickness and Kelvin with half thickness

Similar patterns are observed in the IsoTruss structure. The convergence of KPI_1 is signif-

icantly faster, approximately 80% or 208 s less than the reference case. Again, this represents a substantial increase in performance, but it also leads to lower maximum values. The double thickness case exhibits a 30% reduction in the maximum value of KPI_1 and a 13% decrease in the maximum value of KPI_2.

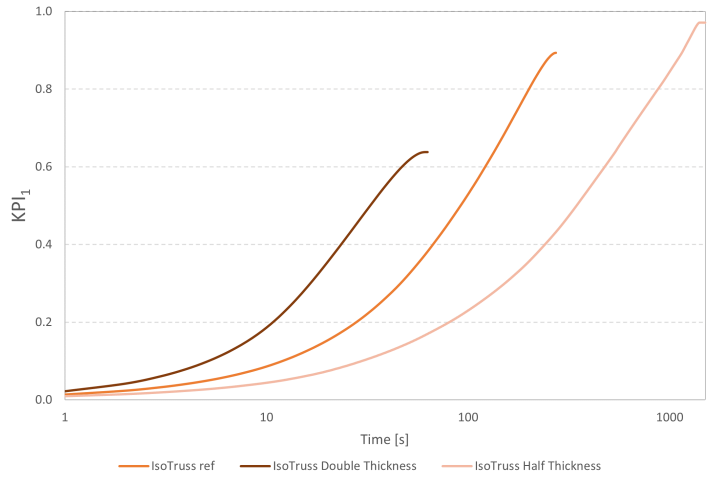

Figure 5.14: KPI_1 comparison between IsoTruss reference, IsoTruss with double thickness and IsoTruss with half thickness

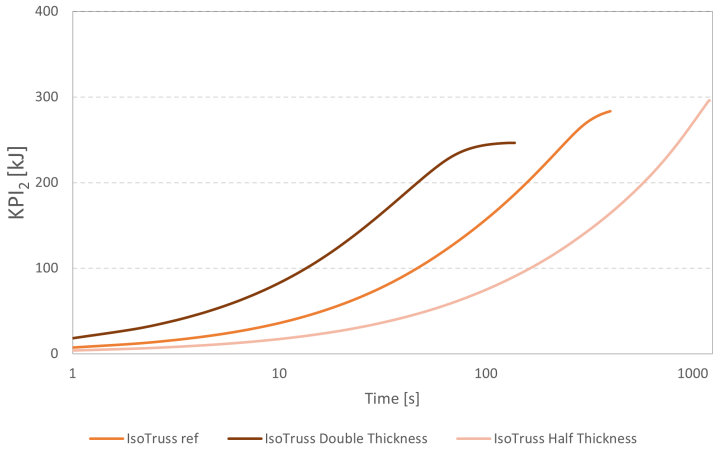

Figure 5.15: KPI_2 comparison between IsoTruss reference, IsoTruss with double thickness and IsoTruss with half thickness

The Gyroid structure follows a similar trend. Increasing the thickness results in a 52% increase in the convergence rate of KPI_1. While this represents a considerable improvement, the maximum value of KPI_2 for the double thickness case is approximately 7% lower than that of the reference case.

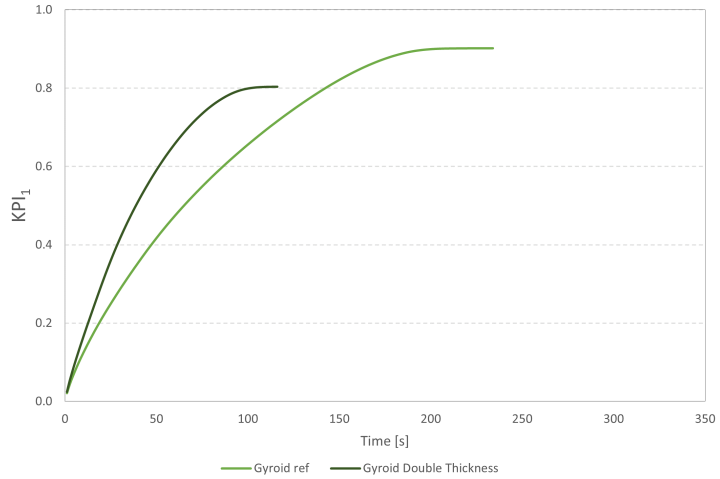

Figure 5.16: KPI_1 comparison between Gyroid reference, Gyroid with double thickness

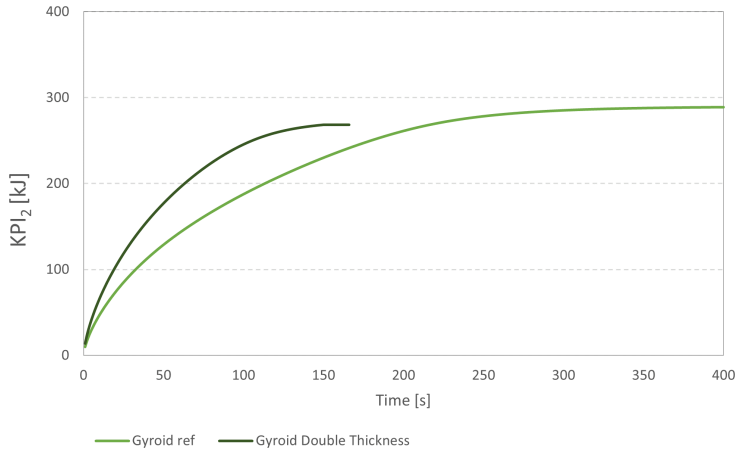

Figure 5.17: KPI_2 comparison between Gyroid reference, Gyroid with double thickness

To summarize the findings, increasing the thickness enhances performance across all cell types. However, this improvement comes at the expense of heat storage capacity. The decrease in heat storage capacity is primarily attributed to the reduction in PCM volume across the configurations. The extent of PCM volume reduction is closely linked to the decrease in KPI_2. Configurations with larger reductions in PCM volume experience greater decreases in heat storage capacity. Additionally, the rate of convergence may also be influenced by PCM volume. Configurations showing higher decreases in PCM volume exhibit the highest increases in convergence rate. These observations highlight the interplay between thickness, PCM volume, and performance.

5.3.2 Decreasing thickness

Decreasing the thickness yields new parameter values for each structure: 0.465 mm and 0.390 mm for the Kelvin and IsoTruss structures, respectively. Consequently, the properties of each structure undergo changes. The PCM volume increases by 8% for both cell types, while the surface area decreases by 2% for the Kelvin structure and 16% for the IsoTruss structure. The reduced thickness values correspond to a porosity of approximately 97%, indicating that only 3% of the structure consists of matrix material.

Examining the results for the Kelvin configuration, there is a significant change in the convergence rate of KPI_1. Decreasing the thickness causes the maximum value of KPI_1 to be reached 275% slower compared to the reference case. This translates to a difference of 839 s in reaching this value. By the time the reference case finishes converging to its maximum KPI_1, the half thickness case has only achieved a KPI_1 value of 0.45. Eventually, due to its larger porosity, the half thickness case surpasses the reference case in terms of KPI_1 value. As expected, the convergence of KPI_2 is significantly slower for the half thickness case, but it ultimately reaches a higher value primarily due to the larger porosity. KPI_2 is 14% larger in the half thickness case, resulting in a 14% increase in heat storage capacity. However, this increase comes at the cost of a 275% decrease in performance for this configuration.

Moving on to the IsoTruss configuration, a similar effect is observed. The convergence rate of KPI_1 is significantly slower for the half thickness case, around 418% or 1122 s. This represents a substantial decrease in performance for KPI_1. Similar to the Kelvin configuration, by the time the reference case completes its convergence, the half thickness case has reached a KPI_1 value of 0.42. It eventually surpasses the reference case in terms of KPI_1 value due to its higher porosity. The convergence rate of KPI_2 is also significantly slower for the half thickness case, but it eventually reaches a larger value, indicating a 4% increase in heat storage capacity. In summary, decreasing the thickness results in a 4% increase in heat storage capacity but also a 418% decrease in convergence rate.

An interesting finding emerges from this parameterization. Despite both structures exhibiting comparable porosity, transitioning from 90% porosity to 97%, they behave differently when compared to the results of the reference simulations where IsoTruss was shown to outperform the Kelvin structure. In this case, however, the opposite occurs. Not only does the Kelvin structure outperform the IsoTruss structure, but the IsoTruss structure also fails to increase heat storage capacity to the same extent as the Kelvin structure, despite the identical change in porosity. This discrepancy is quite surprising, and currently, there is no definitive explanation for this phenomenon. Overall it seems that decreasing thickness causes a huge decrease in convergence rate despite increasing the heat storage capacity.

5.4 Impact from surface area variation

Surface area typically plays a crucial role in heat transfer, and it is reasonable to expect that an increase in surface area would result in a higher heat transfer rate for a given structure. While surface area was not directly altered in this study, it was indirectly affected by varying the input variables. This indirect manipulation of surface area raises an interesting question: if different surface area values are stacked up for the same cell design, does it have an impact on KPI_1 or KPI_2? As shown before, ranking structures based on their KPI_2 values outputs the same result as ranking them by KPI_1. Due to this, representing only one of these KPI is enough to understand how surface area plays a role in the system's performance.

By making use of Tables 4.1, 4.2 and 4.3 the cases can be ordered from highest to lowest surface area as follows: double cell, double thickness, reference, half cell, and half thickness.

Contrary to expectations, the double cell case with higher thickness does not outperform every single structure. Surprisingly, it is outperformed by the double thickness case in terms of convergence rate to KPI_1. Also despite having a similar volume as the reference case and the half-cell case but a higher surface area it only just slightly outperforms them. In fact, when considering the order of convergence rate for KPI_1, it goes as follows: double thickness, double cell, half cell, reference and half thickness. For the Gyroid configuration, the order for convergence rate is slightly different: double thickness, gyroid ref, half cell, double cell. This ordering is quite different from the one based on surface area and shows that this parameter does not show a high correlation with the systems convergence rate or KPI_1 value. A visualization on how the diferent cases surface area stack up against each other can be viewed in Figure 5.18, 5.19 and 5.20.

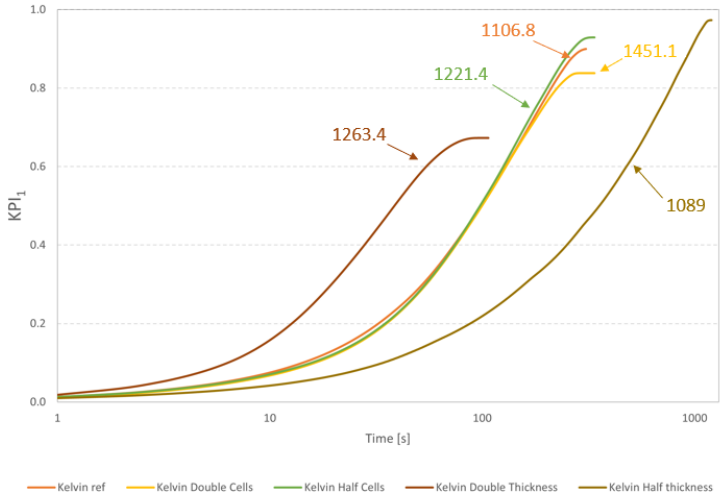

Figure 5.18: KPI_1 comparison for Kelvin configuration highlighting surface area values for each case

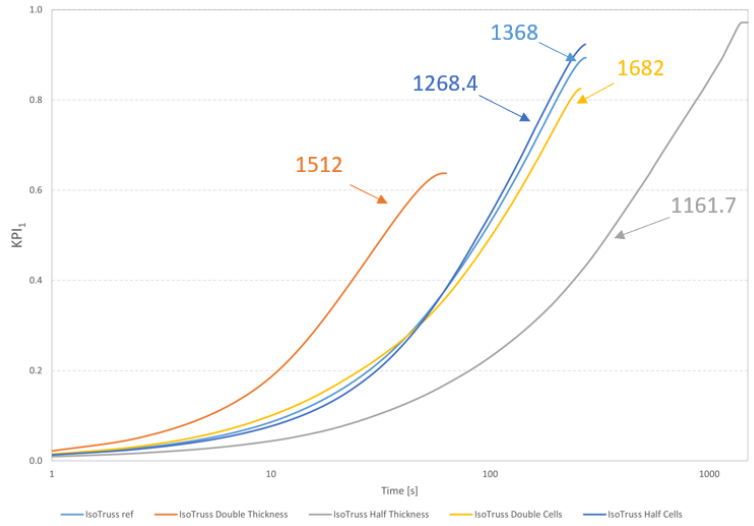

Figure 5.19: KPI_1 comparison for IsoTruss configuration highlighting surface area values for each case

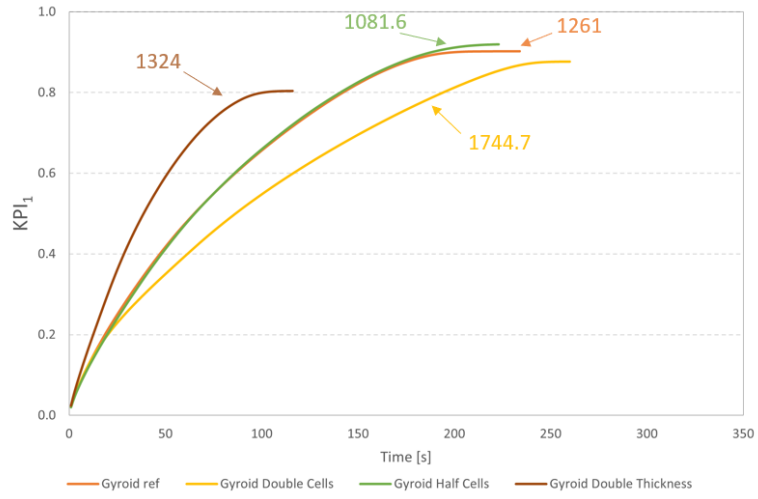

Figure 5.20: KPI_1 comparison for Gyroid configuration highlighting surface area values for each case

Chapter 6

Conclusions and Future Works

6.1 Conclusions

First and foremost, it is essential to reflect on whether the objective of this dissertation has been accomplished. The primary aim of this document was to draw conclusions regarding the best design and configuration of the matrix plus PCM system. While considerable efforts have been dedicated to this pursuit, it is important to acknowledge that the objective has only been partially achieved.

Throughout this dissertation, an extensive investigation was conducted to study and compare the effects of different parameters on various structures of the matrix plus PCM system. Although valuable insights have been gained from this line of work, an optimal configuration that fully meets the predetermined criteria could not be ultimately identified. It should be noted, however, that the conclusions drawn from this study are not without significance. The findings provide valuable information and lay the groundwork for further advancements in the field.

To achieve the desired optimal configuration, a more comprehensive exploration of parameters and additional analyses would have been necessary. The limitations encountered in this study point to the need for further research and development in the area of matrix plus PCM system design and configuration. By acknowledging these limitations, we open up new avenues for future investigations, enabling researchers to build upon this study's foundation and address the gaps and challenges encountered.

Regarding the thickness variation, increasing the thickness of the structures enhances performance and convergence rate, but at the expense of heat storage capacity due to a reduction in PCM volume. On the other hand, decreasing the thickness increases PCM volume and porosity, leading to slower convergence but higher heat storage capacity. The observed discrepancies between the Kelvin and IsoTruss structures in terms of heat storage capacity require further investigation to fully understand their underlying reasons.

In the analysis of cell size variation, decreasing the cell size has varying effects depending on the configuration. While it improves the convergence rate for the Kelvin and IsoTruss structures, there is a decrease in heat storage capacity. Surprisingly, the Gyroid structure shows a decrease in convergence rate, deviating from the observed trend. Increasing the cell size has a minor positive effect on performance and heat storage capacity across the structures.

From the observed results, the configuration that stands out compared to the other evaluated configurations, in terms of convergence rate to KPI_1 and also KPI_2, seems to be the Gyroid cell-based configuration with double the amount of thickness. This configuration also exhibits

a significant increase in performance for a smaller decrease in heat storage capacity. This is somewhat in accordance with expectations. As discussed in Chapter 2, TPMS cells, including the Gyroid, show promising results in terms of heat transfer enhancement in lattice systems. These findings confirm the findings in the referenced base study [9].

Overall, the optimization of cell size and thickness parameters is crucial for achieving optimal performance and heat storage capacity in PCM and metal lattice systems. The findings emphasize the need for careful parameter selection and a systematic approach to parameter optimization. The developed simulation methodology and the insights gained from this research contribute to the advancement of thermal energy storage applications using PCM and metal lattice systems.

It is also interesting to see how the same modification to the initial parameters has a different impact on the system's properties, depending on cell type. It has been shown that a higher variance in matrix volume does not translate to a higher change in surface area. In fact, these properties appear to not show any type of correlation. Surface area appears to have a higher link to the cell type and its material distribution along the structure. Furthermore surface area does not display a strong correlation with KPI_1, KPI_2 or convergence rate to these metrics.

Further research is required to fully understand the observed discrepancies and optimize these systems based on the findings. By refining the understanding of the interplay between parameters and system behavior, more efficient and sustainable energy storage systems can be designed and implemented.

6.2 Future Works

Based on the analysis and conclusions presented in this dissertation, several potential future research directions and areas for further investigation can be recommended:

- Optimal cell size and thickness determination: Conduct a comprehensive study to determine the optimal combination of cell size and thickness for each structure configuration. This involves exploring a wider range of cell sizes and thicknesses and evaluating their individual and combined impact on performance indicators and heat storage capacity. The goal is to find the cell size and thickness combination that maximizes both performance and heat storage efficiency.

- Advanced performance metrics: Explore additional performance metrics beyond the ones used in this study, such as temperature uniformity, response time, and energy transfer efficiency. This provides a more comprehensive evaluation of the structures' behavior and enables better comparisons between different configurations, considering both cell size and thickness variations.

- Experimental validation: Conduct experimental studies to validate the findings from the numerical simulations, considering variations in both cell size and thickness. Real-world experiments provide insights into the actual performance of the structures and validate the accuracy of the numerical models. Additionally, experimental data can be used to refine and improve the numerical models for better prediction and optimization, taking into account the impact of both cell size and thickness variations.

- Multiscale analysis: Explore the behavior of the structures at different scales, considering variations in both cell size and thickness. Investigate how variations in cell size and thick-

ness affect heat transfer and storage at different scales and analyze the interplay between microstructural properties and overall system performance. This multiscale analysis provides a comprehensive understanding of the impact of both cell size and thickness on the performance and heat storage capacity of the structures.

- Extended parameter variation: In addition to cell size and thickness, investigate the effects of other parameters on the structures' performance, considering their interaction. This includes variations in the material properties of the PCM and matrix and different boundary conditions among others. Analyze how these variations interact with cell size and thickness and explore their combined influence on performance and heat storage capacity.

By addressing these future research directions, a deeper understanding of the impact of cell size, thickness, and other parameters on the performance and heat storage capacity of the structures can be achieved. This knowledge contributes to the development of more efficient and optimized designs for TES systems.

Intentionally blank page.

Appendix A

Liquid fraction for cell and thickness variation

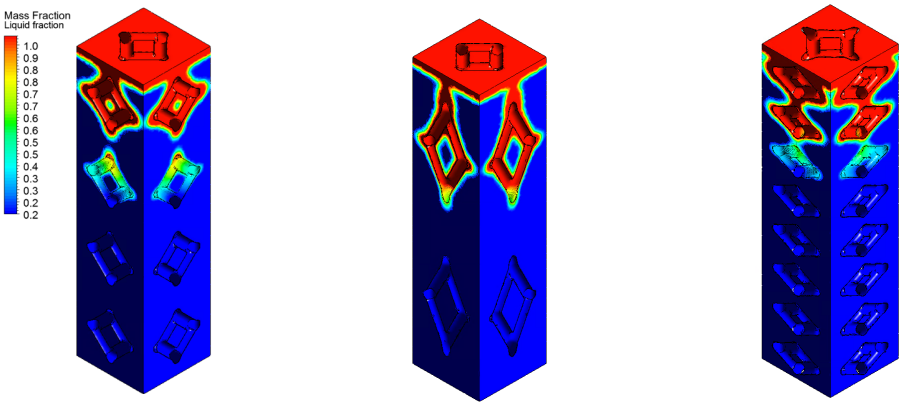

(a) (b) (c)

Figure A.1: PCM liquid fraction at 10s for the $7mm$x$7mm$x$28mm$ structure of (a) Kelvin reference case (b) Kelvin with half the cell number (c) Kelvin with double the cell number

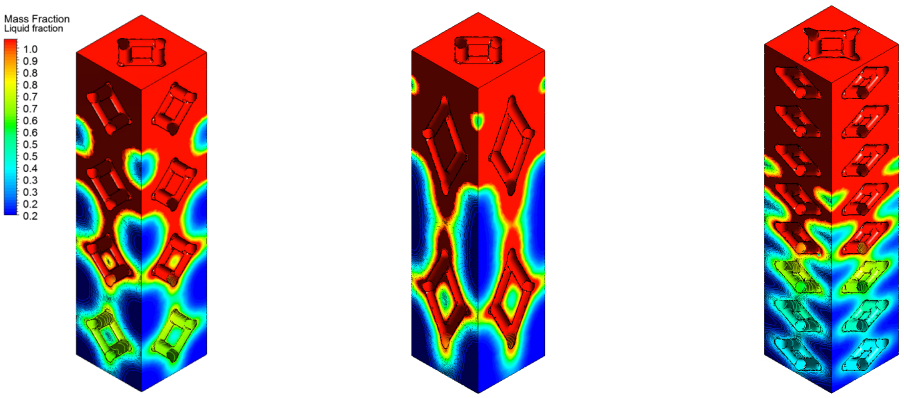

(a) (b) (c)

Figure A.2: PCM liquid fraction at 100s for the $7mm$x$7mm$x$28mm$ structure of (a) Kelvin reference case (b) Kelvin with half the cell number (c) Kelvin with double the cell number

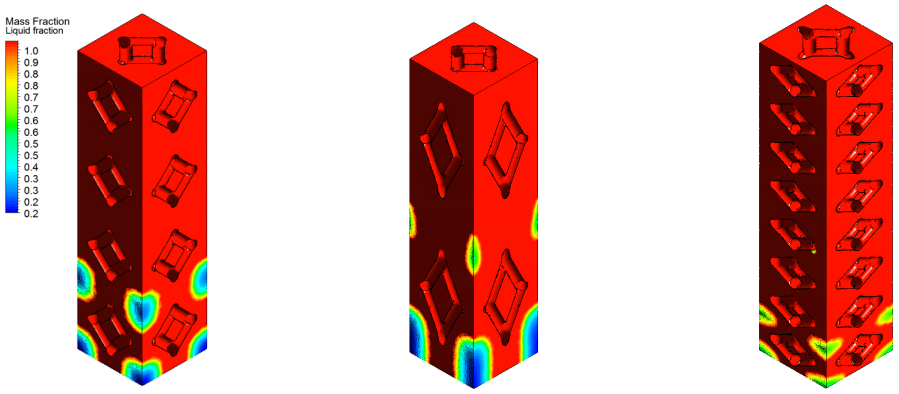

(a) (b) (c)

Figure A.3: PCM liquid fraction at 250s for the $7mm$x$7mm$x$28mm$ structure of (a) Kelvin reference case (b) Kelvin with half the cell number (c) Kelvin with double the cell number

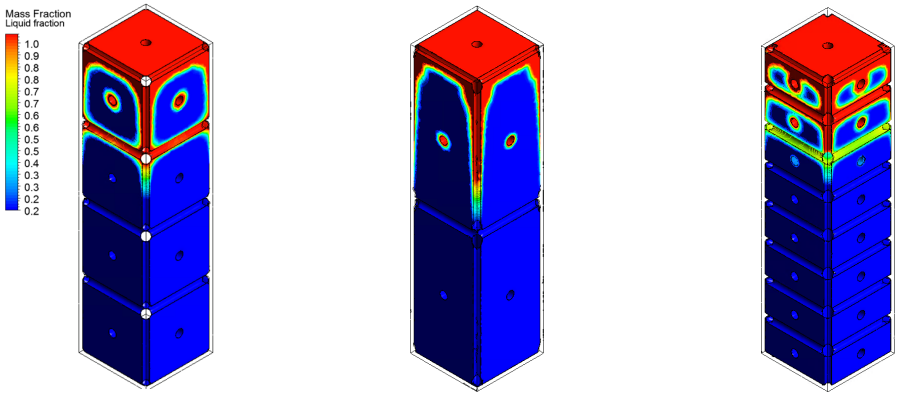

(a) (b) (c)

Figure A.4: PCM liquid fraction at 10s for the $7mm$x$7mm$x$28mm$ structure of (a) IsoTruss reference case (b) IsoTruss with half the number of cells (c) IsoTruss with double the number of cells

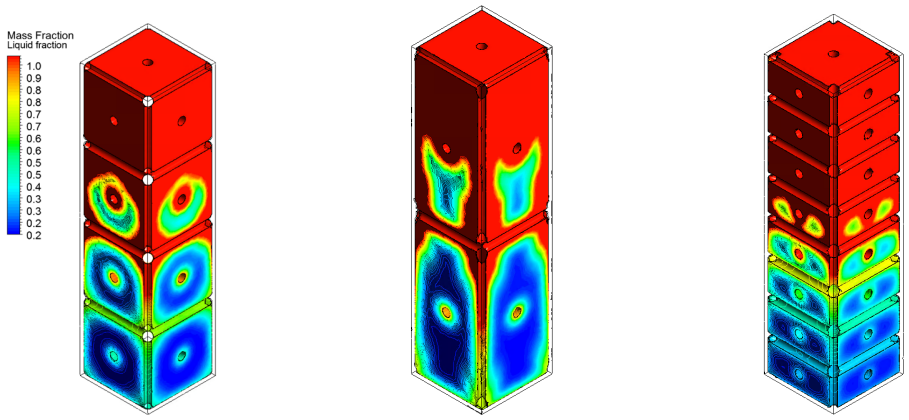

(a) (b) (c)

Figure A.5: PCM liquid fraction at 100s for the $7mm$x$7mm$x$28mm$ structure of (a) IsoTruss reference case (b) IsoTruss with half the number of cells (c) IsoTruss with double the number of cells

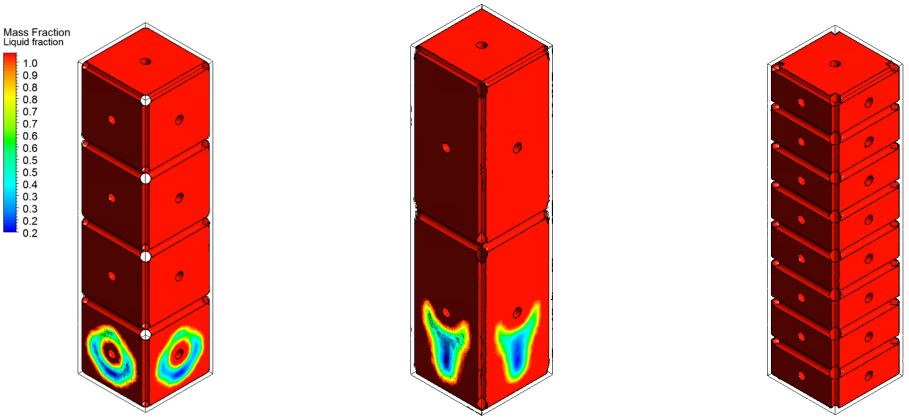

(a) (b) (c)

Figure A.6: PCM liquid fraction at 250s for the $7mm$x$7mm$x$28mm$ structure of (a) IsoTruss reference case (b) IsoTruss with half the number of cells (c) IsoTruss with double the number of cells

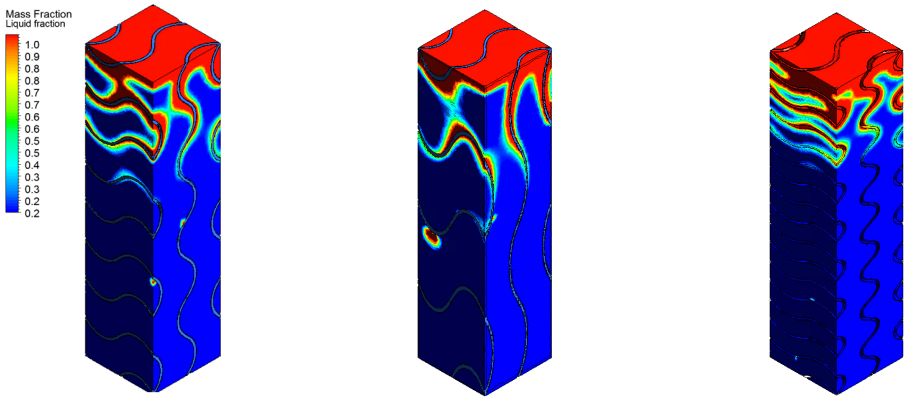

(a) (b) (c)

Figure A.7: PCM liquid fraction at 10s for the $7mm$x$7mm$x$28mm$ structure of (a) Gyroid reference case (b) Gyroid with half the number of cells (c) Gyroid with double the number of cells

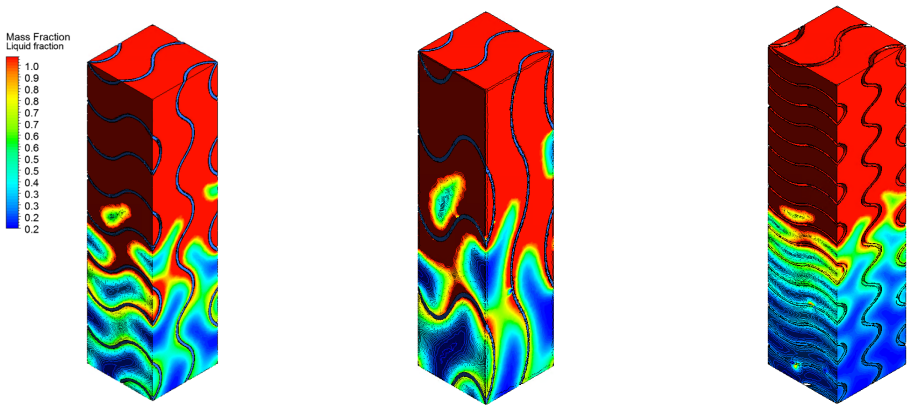

(a) (b) (c)

Figure A.8: PCM liquid fraction at 100s for the $7mm$x$7mm$x$28mm$ structure of (a) Gyroid reference case (b) Gyroid with half the number of cells (c) Gyroid with double the number of cells

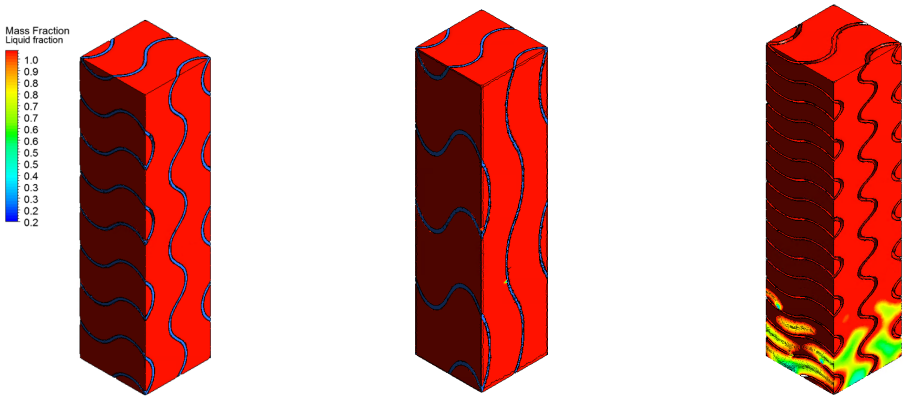

(a) (b) (c)

Figure A.9: PCM liquid fraction at 220s for the $7mm$x$7mm$x$28mm$ structure of (a) Gyroid reference case (b) Gyroid with half the number of cells (c) Gyroid with double the number of cells

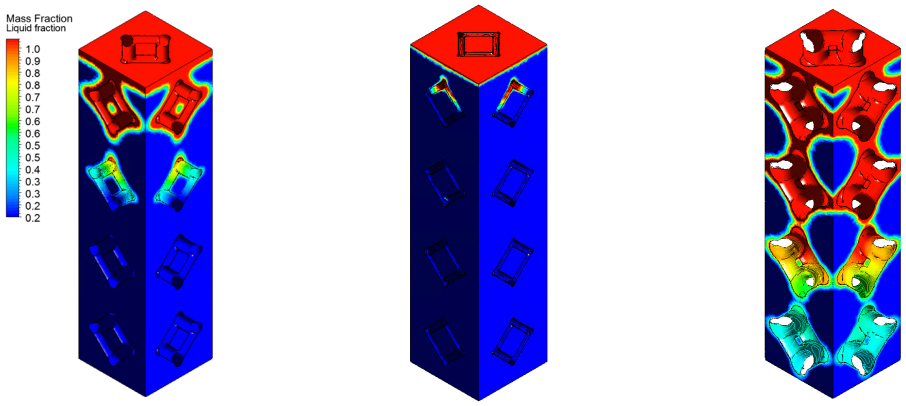

(a) (b) (c)

Figure A.10: PCM liquid fraction at 10s for the $7mm$x$7mm$x$28mm$ structure of (a) Kelvin reference case (b) Kelvin with half thickness (c) Kelvin with double thickness

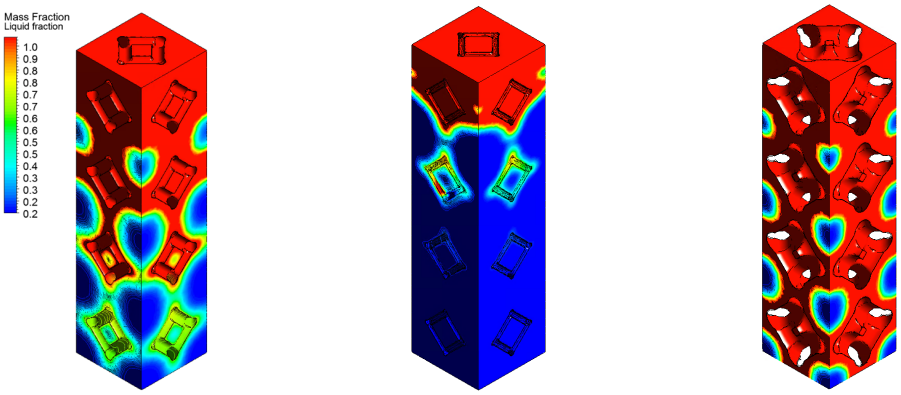

(a) (b) (c)

Figure A.11: PCM liquid fraction at 100s for the $7mm$x$7mm$x$28mm$ structure of (a) Kelvin reference case (b) Kelvin with half thickness and at 50s for (c) Kelvin with double thickness

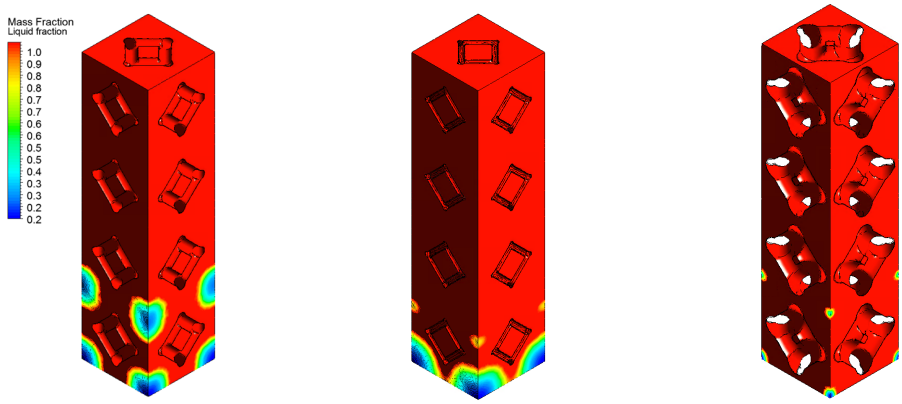

(a) (b) (c)

Figure A.12: PCM liquid fraction at 250s for the $7mm$x$7mm$x$28mm$ structure of (a) Kelvin reference case at 1000s for (b) Kelvin with half thickness and 100s for (c) Kelvin with double thickness

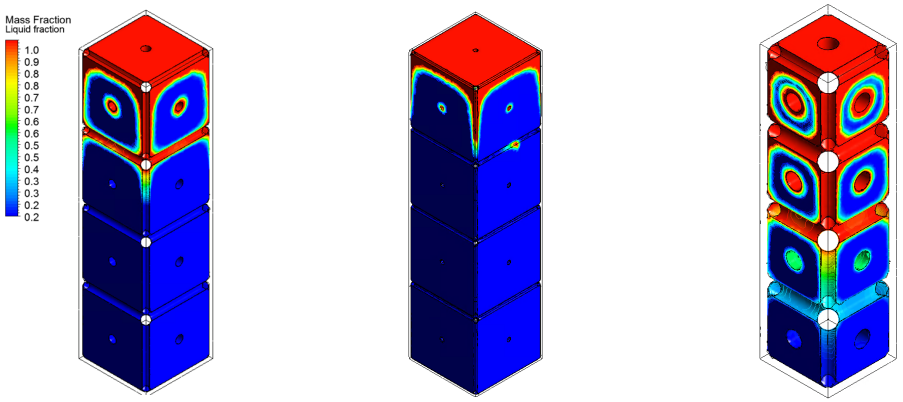

(a) (b) (c)

Figure A.13: PCM liquid fraction at 10s for the $7mm$x$7mm$x$28mm$ structure of (a) IsoTruss reference case (b) IsoTruss with half thickness (c) IsoTruss with double thickness

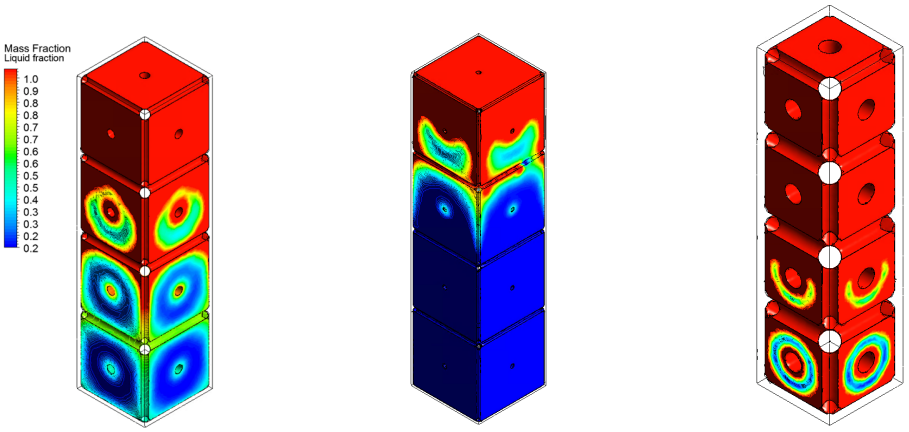

(a) (b) (c)

Figure A.14: PCM liquid fraction at 100s for the $7mm$x$7mm$x$28mm$ structure of (a) IsoTruss reference case (b) IsoTruss with half thickness and 50s for (c) IsoTruss with double thickness

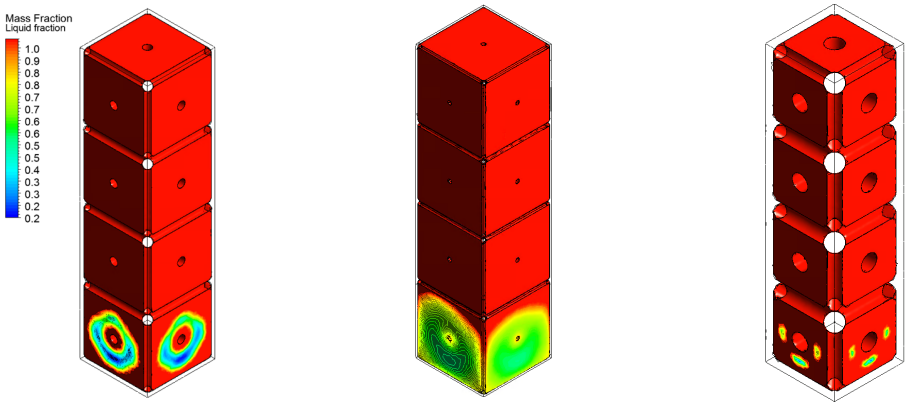

(a) (b) (c)

Figure A.15: PCM liquid fraction at 250s for the $7mm$x$7mm$x$28mm$ structure of (a) IsoTruss reference case 1000s for (b) IsoTruss with half thickness and 60s for (c) IsoTruss with double thickness

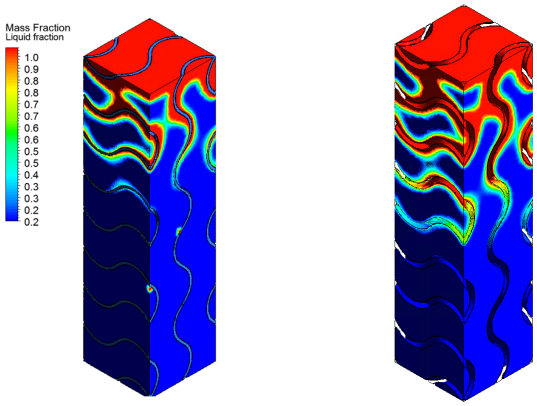

(a) (b)

Figure A.16: PCM liquid fraction at 10s for the $7mm$x$7mm$x$28mm$ structure of (a) Gyroid reference case (b) Gyroid with double thickness

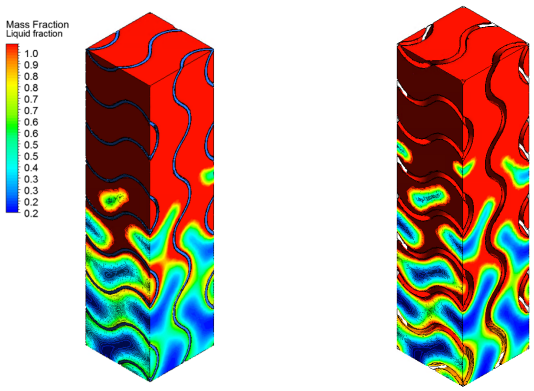

(a) (b)

Figure A.17: PCM liquid fraction at 100s for the $7mm$x$7mm$x$28mm$ structure of (a) Gyroid reference case and 50s for (b) Gyroid with double thickness

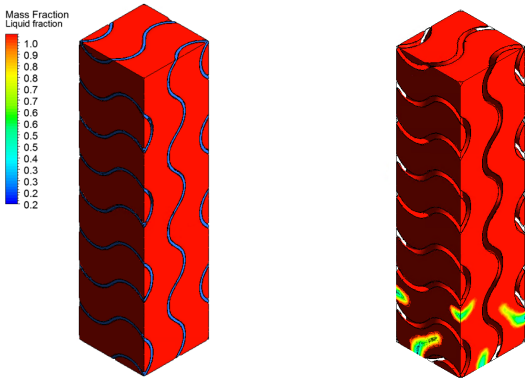

(a) (b)

Figure A.18: PCM liquid fraction at 220s for the $7mm$x$7mm$x$28mm$ structure of (a) Gyroid reference case and 100s for (b) Gyroid with double thickness

Intentionally blank page.

References

[1] A. F. Regin, S. C. Solanki, and J. S. Saini, "Heat transfer characteristics of thermal energy storage system using pcm capsules: A review," pp. 2438–2458, 2008.

[2] T. ur Rehman, H. M. Ali, M. M. Janjua, U. Sajjad, and W. M. Yan, "A critical review on heat transfer augmentation of phase change materials embedded with porous materials/foams," pp. 649–673, 6 2019.

[3] M. S. Mahdi, H. B. Mahood, A. A. Alammar, and A. A. Khadom, "Numerical investigation of pcm melting using different tube configurations in a shell and tube latent heat thermal storage unit," *Thermal Science and Engineering Progress*, vol. 25, 10 2021.

[4] A. N. Desai, A. Gunjal, and V. K. Singh, "Numerical investigations of fin efficacy for phase change material (pcm) based thermal control module," *International Journal of Heat and Mass Transfer*, vol. 147, 2 2020.

[5] N. I. Ibrahim, F. A. Al-Sulaiman, S. Rahman, B. S. Yilbas, and A. Z. Sahin, "Heat transfer enhancement of phase change materials for thermal energy storage applications: A critical review," pp. 26–50, 2017.

[6] K. Lafdi, O. Mesalhy, and S. Shaikh, "Experimental study on the influence of foam porosity and pore size on the melting of phase change materials," *Journal of Applied Physics*, vol. 102, 2007.

[7] Z. A. Qureshi, S. A. B. Al-Omari, E. Elnajjar, O. Al-Ketan, and R. A. Al-Rub, "Architected lattices embedded with phase change materials for thermal management of high-power electronics: A numerical study," *Applied Thermal Engineering*, vol. 219, 1 2023.

[8] I. Sarbu and A. Dorca, "Review on heat transfer analysis in thermal energy storage using latent heat storage systems and phase change materials," pp. 29–64, 1 2019.

[9] Z. A. Qureshi, S. A. B. Al-Omari, E. Elnajjar, O. Al-Ketan, and R. A. Al-Rub, "Using triply periodic minimal surfaces (tpms)-based metal foams structures as skeleton for metal-foam-pcm composites for thermal energy storage and energy management applications," *International Communications in Heat and Mass Transfer*, vol. 124, 5 2021.

[10] "World energy outlook 2022," 2. [Online]. Available: www.iea.org/t&c/

[11] C. N. Elias and V. N. Stathopoulos, "A comprehensive review of recent advances in materials aspects of phase change materials in thermal energy storage," vol. 161. Elsevier Ltd, 2019, pp. 385–394.

[12] H. Mehling and L. F. Cabeza, *Heat and cold storage with PCM*. Springer Berlin Heidelberg, 2008. [Online]. Available: http://link.springer.com/10.1007/978-3-540-68557-9

[13] K. Pielichowska and K. Pielichowski, "Phase change materials for thermal energy storage," pp. 67–123, 2014.

[14] Z. Ling, Z. Zhang, G. Shi, X. Fang, L. Wang, X. Gao, Y. Fang, T. Xu, S. Wang, and X. Liu, "Review on thermal management systems using phase change materials for electronic components, li-ion batteries and photovoltaic modules," pp. 427–438, 2014.

[15] S. A. Khateeb, S. Amiruddin, M. Farid, J. R. Selman, and S. Al-Hallaj, "Thermal management of li-ion battery with phase change material for electric scooters: Experimental validation," *Journal of Power Sources*, vol. 142, pp. 345–353, 3 2005.

[16] T. Y. Kim, B. S. Hyun, J. J. Lee, and J. Rhee, "Numerical study of the spacecraft thermal control hardware combining solid-liquid phase change material and a heat pipe," *Aerospace Science and Technology*, vol. 27, pp. 10–16, 6 2013.

[17] D. V. Hale, M. J. Hoover, and M. J. O'neill, "Nasa contractor report nasa cr-51363 phase change materials handbook," 1971.

[18] F. Salaün, E. Devaux, S. Bourbigot, and P. Rumeau, "Development of phase change materials in clothing part i: Formulation of microencapsulated phase change," *Textile Research Journal*, vol. 80, pp. 195–205, 2010.

[19] Y. Lu, X. Xiao, J. Fu, C. Huan, S. Qi, Y. Zhan, Y. Zhu, and G. Xu, "Novel smart textile with phase change materials encapsulated core-sheath structure fabricated by coaxial electrospinning," *Chemical Engineering Journal*, vol. 355, pp. 532–539, 1 2019.

[20] M. C. Browne, B. Norton, and S. J. McCormack, "Phase change materials for photovoltaic thermal management," pp. 762–782, 2015.

[21] K. Du, J. Calautit, P. Eames, and Y. Wu, "A state-of-the-art review of the application of phase change materials (pcm) in mobilized-thermal energy storage (m-tes) for recovering low-temperature industrial waste heat (iwh) for distributed heat supply," pp. 1040–1057, 5 2021.

[22] S. A. Memon, "Phase change materials integrated in building walls: A state of the art review," pp. 870–906, 2014.

[23] M. Hagenau and M. Jradi, "Dynamic modeling and performance evaluation of building envelope enhanced with phase change material under danish conditions," *Journal of Energy Storage*, vol. 30, 8 2020.

[24] M. Mu, S. Zhang, S. Yang, and Y. Wang, "Phase change materials applied in agricultural greenhouses," 5 2022.

[25] J. Yao, P. Zhu, L. Guo, L. Duan, Z. Zhang, S. Kurko, and Z. Wu, "A continuous hydrogen absorption/desorption model for metal hydride reactor coupled with pcm as heat management and its application in the fuel cell power system," *International Journal of Hydrogen Energy*, vol. 45, pp. 28 087–28 099, 10 2020.

[26] A. P. Sasmito, T. Shamim, and A. S. Mujumdar, "Passive thermal management for pem fuel cell stack under cold weather condition using phase change materials (pcm)," *Applied Thermal Engineering*, vol. 58, pp. 615–625, 2013.

[27] M. J. Huang, "The effect of using two pcms on the thermal regulation performance of bipv systems," *Solar Energy Materials and Solar Cells*, vol. 95, pp. 957–963, 3 2011.

[28] X. Guo, H. Wei, X. He, M. He, and D. Yang, "Integrating phase change material in building envelopes combined with the earth-to-air heat exchanger for indoor thermal environment regulation," *Building and Environment*, vol. 221, 8 2022.

[29] P. T. Sardari, D. Grant, D. Giddings, G. S. Walker, and M. Gillott, "Composite metal foam/pcm energy store design for dwelling space air heating," *Energy Conversion and Management*, vol. 201, 12 2019.

[30] C. Veerakumar and A. Sreekumar, "Phase change material based cold thermal energy storage: Materials, techniques and applications - a review," pp. 271–289, 7 2016.

[31] P. Graça, "ModelaÇÃo e caracterizaÇÃo tÉrmica de materiais de mudanÇa de fase para soluÇÕes de aquecimento ambiente," 2022.

[32] A. Kumar and S. K. Saha, "Latent heat thermal storage with variable porosity metal matrix: A numerical study," *Renewable Energy*, vol. 125, pp. 962–973, 9 2018.

[33] Z. A. Qureshi, E. Elnajjar, O. Al-Ketan, R. A. Al-Rub, and S. B. Al-Omari, "Heat transfer performance of a finned metal foam-phase change material (fmf-pcm) system incorporating triply periodic minimal surfaces (tpms)," *International Journal of Heat and Mass Transfer*, vol. 170, 5 2021.

[34] S. Mahmoud, A. Tang, C. Toh, R. AL-Dadah, and S. L. Soo, "Experimental investigation of inserts configurations and pcm type on the thermal performance of pcm based heat sinks," *Applied Energy*, vol. 112, pp. 1349–1356, 2013.

[35] T. Brahim, M. H. Dhaou, and A. Jemni, "Theoretical and experimental investigation of plate screen mesh heat pipe solar collector," *Energy Conversion and Management*, vol. 87, pp. 428–438, 2014.

[36] K. Nithyanandam and R. Pitchumani, "Computational studies on a latent thermal energy storage system with integral heat pipes for concentrating solar power," *Applied Energy*, vol. 103, pp. 400–415, 2013.

[37] J. M. Mahdi, H. I. Mohammed, E. T. Hashim, P. Talebizadehsardari, and E. C. Nsofor, "Solidification enhancement with multiple pcms, cascaded metal foam and nanoparticles in the shell-and-tube energy storage system," *Applied Energy*, vol. 257, 1 2020.

[38] E. B. S. Mettawee and G. M. Assassa, "Thermal conductivity enhancement in a latent heat storage system," *Solar Energy*, vol. 81, pp. 839–845, 7 2007.

[39] J. M. Khodadadi and S. F. Hosseinizadeh, "Nanoparticle-enhanced phase change materials (nepcm) with great potential for improved thermal energy storage," *International Communications in Heat and Mass Transfer*, vol. 34, pp. 534–543, 5 2007.

[40] S. Jegadheeswaran and S. Pohekar, "Energy analysis of particle dispersed latent heat thermal storage system for solar water heaters," *Jornal of Renewable and Sustainable Energy*, vol. 2, 2010.

[41] Z. Youssef, A. Delahaye, L. Huang, F. Trinquet, L. Fournaison, C. Pollerberg, and C. Doetsch, "State of the art on phase change material slurries," *Energy Conversion and Management*, vol. 65, pp. 120–132, 1 2013.

[42] L. Huang, M. Petermann, and C. Doetsch, "Evaluation of paraffin/water emulsion as a phase change slurry for cooling applications," *Energy*, vol. 34, pp. 1145–1155, 2009.

[43] C. Veerakumar and A. Sreekumar, "Phase change material based cold thermal energy storage: Materials, techniques and applications - a review," pp. 271–289, 7 2016.

[44] Z. Deng, X. Liu, C. Zhang, Y. Huang, and Y. Chen, "Melting behaviors of pcm in porous metal foam characterized by fractal geometry," *International Journal of Heat and Mass Transfer*, vol. 113, pp. 1031–1042, 2017.

[45] Goodfellow, "Metal—thermal catalogue," 2015.

[46] Z. Li and Z. G. Wu, "Numerical study on the thermal behavior of phase change materials (pcms) embedded in porous metal matrix," *Solar Energy*, vol. 99, pp. 172–184, 1 2014.

[47] Y. Zhong, Q. Guo, S. Li, J. Shi, and L. Liu, "Heat transfer enhancement of paraffin wax using graphite foam for thermal energy storage," *Solar Energy Materials and Solar Cells*, vol. 94, pp. 1011–1014, 6 2010.

[48] Y. Zhong, S. Li, X. Wei, Z. Liu, Q. Guo, J. Shi, and L. Liu, "Heat transfer enhancement of paraffin wax using compressed expanded natural graphite for thermal energy storage," *Carbon*, vol. 48, pp. 300–304, 1 2010.

[49] Z. G. Wu and C. Y. Zhao, "Experimental investigations of porous materials in high temperature thermal energy storage systems," *Solar Energy*, vol. 85, pp. 1371–1380, 7 2011.

[50] M. P. Behera, T. Dougherty, and S. Singamneni, "Conventional and additive manufacturing with metal matrix composites: A perspective," vol. 30. Elsevier B.V., 2019, pp. 159–166.

[51] J. Banhart, "Metal foams: Production and stability," pp. 781–794, 9 2006.

[52] S. Catchpole-Smith, R. R. Sélo, A. W. Davis, I. A. Ashcroft, C. J. Tuck, and A. Clare, "Thermal conductivity of tpms lattice structures manufactured via laser powder bed fusion," *Additive Manufacturing*, vol. 30, 12 2019.

[53] Z. A. Qureshi, S. A. B. A. Omari, E. Elnajjar, F. Mahmoud, O. Al-Ketan, and R. A. Al-Rub, "Thermal characterization of 3d-printed lattices based on triply periodic minimal surfaces embedded with organic phase change material," *Case Studies in Thermal Engineering*, vol. 27, 10 2021.

[54] S. Catchpole-Smith, R. R. Sélo, A. W. Davis, I. A. Ashcroft, C. J. Tuck, and A. Clare, "Thermal conductivity of tpms lattice structures manufactured via laser powder bed fusion," *Additive Manufacturing*, vol. 30, 12 2019.

[55] K. Merlin, D. Delaunay, J. Soto, and L. Traonvouez, "Heat transfer enhancement in latent heat thermal storage systems: Comparative study of different solutions and thermal contact investigation between the exchanger and the pcm," *Applied Energy*, vol. 166, pp. 107–116, 3 2016.

[56] "ntopology ntop software," 11 2022.

[57] "Techdata_$rt42_en_09102020.''$